Simulated responses of soil carbon to climate change in CMIP6 Earth System Models: the role of false priming

Rebecca M. Varney[1], Sarah E. Chadburn[1], Eleanor J. Burke[2], Andy J. Wiltshire[2, 3], and Peter M. Cox[1, 3]

[1]Department of Mathematics and Statistics, Faculty of Environment, Science and Economy, University of Exeter, Laver Building, North Park Road, Exeter, EX4 4QE, UK
[2]Met Office Hadley Centre, FitzRoy Road, Exeter, EX1 3PB, UK
[2]Global Systems Institute, University of Exeter, Laver Building, North Park Road, Exeter, EX4 4QE, UK

Correspondence: Rebecca M. Varney (r.varney@exeter.ac.uk)

Abstract. Reliable estimates of soil carbon change are required to determine the carbon budgets consistent with the Paris Agreement climate targets. This study evaluates projections of soil carbon during the 21st century in CMIP6 Earth System Models (ESMs) under a range of atmospheric composition scenarios. In general, we find a reduced spread of changes in global soil carbon (ΔC_s) in CMIP6 compared to the previous CMIP5 model generation. However, similar reductions were not seen in the derived contributions to ΔC_s due to both increases in plant Net Primary Productivity (NPP, named $\Delta C_{s,NPP}$) and reductions in the effective soil carbon turnover time (τ_s, named $\Delta C_{s,\tau}$). Instead, we find a strong relationship across the CMIP6 models between these NPP and τ_s components of ΔC_s, with more positive values of $\Delta C_{s,NPP}$ being correlated with more negative values of $\Delta C_{s,\tau}$. We show that ~~this emergent relationship is the result~~ the concept of 'false priming' is likely to be contributing to this emergent relationship, which leads to a decrease in the effective soil carbon turnover time as a direct result of NPP increase and occurs when the rate of increase of NPP is relatively fast compared to the slower timescales of a multipool soil carbon model. ~~The inclusion of more~~ This finding suggests that the structure of soil carbon models ~~with multiple pools~~ within ESMs in CMIP6 ~~compared to CMIP5, therefore seems to have~~ has likely contributed towards the reduction in the overall model spread in future soil carbon projections since CMIP5.

1 Introduction

The response of soil carbon to human-induced climate change represents one of the greatest uncertainties in determining future atmospheric CO_2 concentrations (Canadell et al., 2021). Global soil carbon stocks contain at least 3 times more carbon than present atmospheric concentrations and is the largest store of carbon on the land surface of Earth (Jackson et al., 2017). The land surface has been a carbon sink throughout the 20th century and is estimated to be currently absorbing about 30% of current CO_2 emissions (Friedlingstein et al., 2022). However, the long-term response of soil carbon is uncertain due to large stocks which are known to be particularly sensitive to changes in CO_2 and the subsequent global warming (Cox et al., 2000). For example, permafrost thaw under climate change has the potential to release significant amounts of carbon into the atmosphere over a short period of time with increased warming, representing a significant feedback within the climate system (Schuur

et al., 2022; Hugelius et al., 2020; Burke et al., 2017). Therefore, quantifying the future response of soil carbon ~~to increased CO_2~~ under future changes to climate is vital in determining the long-term potential land carbon storage.

Soil carbon storage in the future will be determined by the net response of changes in land-atmosphere carbon exchange under increased anthropogenic CO_2. The carbon fluxes which control the fate of global soil carbon stocks are known to be sensitive to changes in climate, and therefore result in soil carbon driven feedbacks to climate change (Canadell et al., 2021). The overall effect of climate change on soil carbon is not very well constrained due to competing feedbacks (Arora et al., 2020, 2013). These include both the negative feedback due to the CO_2 fertilisation effect resulting in increased absorption of carbon by the land surface (Schimel et al., 2015), and the positive climate feedback due to increased carbon losses via soil respiration ~~(Crowther et al., 2016)~~(Crowther et al., 2016; Van Gestel et al., 2018). The balance between these effects will determine the future response of soil carbon stocks under a changing climate (Friedlingstein et al., 2006).

This study assumes Net Primary Productivity (NPP) represents the input flux of carbon to the ~~soil~~system, and is defined as the net rate of accumulation of carbon by vegetation arising from photosynthesis minus the loss from plant respiratory fluxes (Todd-Brown et al., 2014, 2013). In the absence of nutrient and moisture limitations (Wieder et al., 2015b; Green et al., 2019), NPP is projected to increase under increased atmospheric CO_2 due to the CO_2 ~~fertilization~~ fertilisation effect, which can result in an increased soil carbon storage through increased litter (Schimel et al., 2015). Heterotrophic respiration (R_h) is assumed to represent the output flux of carbon from the soil ~~,~~and is defined as the carbon losses due to decomposition from microbes in the soil. R_h is projected to increase under global warming, ~~where increased global temperatures result in~~ due to an increased rate of microbial decomposition ~~(Varney et al., 2020)~~under warming (Varney et al., 2020), in the absence of significant increases in soil moisture (Sierra et al., 2015; Schmidt et al., 2011). Soil carbon turnover time (τ_s) is defined as the ratio of soil carbon stocks to the output flux of carbon (R_h)~~, where~~ . Global warming alone generally reduces τ_s resulting in carbon residing in the soil for less time and a release of carbon from the soil into the atmosphere (Crowther et al., 2016). The effective soil carbon turnover time can also reduce under increasing litterfall inputs (e.g. due to CO_2 fertilisation of plant growth), because the faster components of the soil increase more quickly than the slower components. The net effect of this is that a higher fraction of the soil carbon is held in the fast pools under increasing litterfall, which reduces the effective soil carbon turnover time - a transient phenomenon known as 'false priming' (Koven et al., 2015).

In this study, CMIP6 Earth System Models (ESMs) are used to predict changes to soil carbon stocks under future climate scenarios with differing magnitudes of climate change (*SSP126*, *SSP245*, *SSP585*; Eyring et al. (2016); O'Neill et al. (2016)). The aim is to evaluate estimates of soil carbon change (ΔC_s) during the 21st century to: (a) quantify the soil carbon driven feedback to climate change, and (b) enable comparisons with the previous generation of CMIP5 ESMs (*RCP2.6*, *RCP4.5*, *RCP8.5*; Taylor et al. (2012); Meinshausen et al. (2011)). Additionally, this study includes analysis of 21st century carbon fluxes to and from the soil, represented by changes in NPP and τ_s, and investigates how these individual terms contribute to the net soil carbon response projected by ESMs. Finally, a simple box model is used to investigate soil carbon change, along with idealised 'C4MIP' simulations which separately model the physiological and climate effects of increasing atmospheric CO_2. Our aim is to distinguish more clearly between the direct and indirect mechanisms of reduced soil carbon turnover times by isolating the effects of false priming in models.

2 Methods

2.1 Earth system models

2.1.1 Future climate scenarios

This study uses output data from 10 CMIP6 ESMs (Eyring et al., 2016): ACCESS-ESM1-5, BCC-CSM2-MR, CanESM5, CESM2, CNRM-ESM2-1, IPSL-CM6A-LR, MIROC-ES2L, MPI-ESM1-2-LR, NorESM2-LM, and UKESM1-0-LL. For comparison between the CMIP generations, output data from 9 CMIP5 ESMs ~~is~~ are also used (Taylor et al., 2012): BNU-ESM, CanESM2, GFDL-ESM2G, GISS-E2-R, HadGEM2-ES, IPSL-CM5A-LR, MIROC-ESM, MPI-ESM-LR, and NorESM1-M. The ESMs included were chosen due to the availability of the data required at the time of analysis (CMIP6: https://esgf-node.llnl.gov/search/cmip6/, last access: 8 April 2022) and CMIP5: (https://esgf-node.llnl.gov/search/cmip5/, last access: 12 April 2022). ~~Specific soil carbon related updates within ESMs from~~

The use of CMIP allows for comparison between ESMs in the different ensemble generations. Table 1 presents key soil carbon ESM information from both CMIP6 and CMIP5 ~~to~~ (adapted from Tables 1 and 2 in Varney et al. (2022)). The Table can be used to identify key ESM updates between CMIP6 and CMIP5, such as: the simulation of interactive nitrogen in CMIP6 (ACCESS-ESM1.5, CESM2, MIROC-ES2L, MPI-ESM1.2-LR, NorESM2-LM and UKESM1-0-LL) compared to CMIP5 (NorESM1-M) and the number of soil carbon pools (dead carbon pools). The ESMs where both CMIP5 and CMIP6 generations are included in ~~Varney et al. (2022) within the 'Earth system models ' section of the Methods,~~ our analysis are: CanESM2 and ~~more general model updates are presented within the 'Model descriptions' section of the Arora et al. (2020) Appendix~~CanESM5, GFDL-ESM2G and GDFL-ESM4, IPSL-CM5A-LR and IPSL-CM6A-LR, MIROC-ESM and MIROC-ES2L, MPI-ESM-LR and MPI-ESM1.2-LR, NorESM1-M and NorESM2-LM, and HadGEM2-ES and UKESM1-0-LL, respectively, where direct comparisons can be made. It is noted that some Land Surface Models within ESMs share similarities (e.g. CESM2 and NorESM2-LM both use the Community Land Model version 5; Arora et al. (2020)).

Within ESMs, specific soil carbon processes are modelled using biogeochemical models which are used to simulate the flow and storage of carbon within the soil. Since early models, both the litter and soil are simulated using separate carbon pools, which are used to represent differing sensitivities of carbon to decomposition and allocation into pools is often dependent on the molecular structure of the litter and the long-term stability (Exbrayat et al., 2013). Early examples of soil carbon models are the grass and agroecosystems dynamic model (CENTURY; Parton et al. (1988)) and the Rothamsted carbon model (ROTH-C; Jenkinson et al. (1991)). Updated variants of these models are still widely used to represent soil carbon decomposition in modern ESMs within CMIP (Arora et al., 2020; Todd-Brown et al., 2018). Table 1 presents the number of soil carbon pools (dead carbon pools) within both CMIP5 and CMIP6 ESMs, which can be used to compare between the ESMs.

The analysis in this study considers 3 future climate scenarios defined by CMIP, which are used to consider different levels of global warming and associated climate policies. The CMIP6 'Shared Socioeconomic Pathways' (SSPs) considered in this study are: *SSP126*, *SSP245*, *SSP585*, which run from 2015 to 2100 (O'Neill et al., 2014; O'Neill et al., 2016). These pathways

are chosen to allow for comparison with the CMIP5 'Representative Concentration Pathways' (RCPs): *RCP2.6*, *RCP4.5* and *RCP8.5*, which run from 2005 to 2100 (Meinshausen et al., 2011). It is noted that the SSP and RCP concentration scenarios are not identical, but they are similar enough to enable helpful comparisons between CMIP5 and CMIP6 projections. For the reference period from which change is calculated, the CMIP *Historical* simulation was considered, where the simulation runs from 1850 to 2005 in CMIP5 and from 1850 to 2015 in CMIP6. A change (Δ) was defined as the difference between the last decade of the 21st century (time-averaged between 2090 and 2100) and the last decade of the CMIP5 historical simulation (time-averaged between 1995-2005), which allows for consistency between the CMIP generations. If a timeseries is considered, the historical reference period (historical simulation time-averaged between 1995-2005) was ~~taken away~~ subtracted from the entire future climate simulation (e.g. *SSP126* minus the historical reference period).

2.1.2 C4MIP experiments

This study also uses model experiments set up by the Coupled Climate-Carbon Cycle Model Intercomparison Project (C4MIP), which are idealised experiments designed to separate the effects of CO_2 increases and climate change on land and ocean carbon stores. In these experiments additional effects such as land-use change, aerosols or non-CO_2 greenhouse gases are not included, and nitrogen deposition is fixed at pre-industrial values (Jones et al., 2016). The ~~experiments~~ use of these experiments allows for a more focused evaluation of soil carbon and related fluxes by isolating sensitivities to CO_2 and associated climate changes (e.g. global temperature changes), as well as removing additional complications in the SSP simulations. The experiments included are: (1) a '*full* 1% CO_2 simulation' (CMIP6 simulation *1pctCO2*), which is a simulation that sees a 1% increase in atmospheric CO_2 per year, starting from pre-industrial concentrations (285 ppm) and running for 150 years (*full* 1% CO_2), (2) a biogeochemically coupled '*BGC* simulation' (CMIP6 simulation *1pctCO2-bgc*), where the 1% CO_2 increase per year only affects the carbon cycle component of the ESM and the radiative code remains at pre-industrial CO_2 values (CO_2 only), and (3) a radiatively coupled '*RAD* simulation' (CMIP6 simulation *1pctCO2-rad*), where the 1% CO_2 increase per year affects only the radiative code and the carbon cycle component on the ESM remains at pre-industrial CO_2 values (climate only). These simulations are used with 10 CMIP6 ESMs for further analysis: ACCESS-ESM1-5, BCC-CSM2-MR, CanESM5, CESM2, GFDL-ESM4, IPSL-CM6A-LR, MIROC-ES2L, MPI-ESM1-2-LR, NorESM2-LM, and UKESM1-0-LL, and ~~where~~ 'here 2xCO_2 ~~'~~ and 4xCO_2 are defined as 70 and 140 years into the simulations, respectively.

2.1.3 Climate variables

Using ESM output variables, soil carbon (C_s) is defined as the sum of carbon stored in soils and surface litter (CMIP variable *cSoil* + CMIP variable *cLitter*). This allows for a more consistent comparison between the models due to differences in how soil carbon and litter carbon are defined. For models that do not report a separate litter carbon pool (*cLitter*), soil carbon is taken to be simply the *cSoil* variable (UKESM1-0-LL in CMIP6, GISS-E2-R and HadGEM2-ES in CMIP5). Spatial C_s is given in units of kg m^{-2}, and global total C_s is given in units of PgC, which are calculated using an area weighted sum (using the model land surface fraction, CMIP variable *sftlf*).

Additionally, ESM output variables were used to define the soil carbon driven climate feedbacks. Net Primary Productivity (NPP, CMIP variable *npp*) is defined as the net carbon assimilated by plants via photosynthesis minus loss due to plant respiration and is used to represent the net carbon input flux to the system. Heterotrophic Respiration (R_h, CMIP variable *rh*) is defined as the microbial respiration within global soils and is used to define an effective global soil carbon turnover time (τ_s), see Equation 1. τ_s (years) is defined as the ratio of mean soil carbon to annual mean heterotrophic respiration (where the mean represents an area weighted global average). Carbon fluxes (NPP and R_h) are considered as area weighted global totals in units of PgC yr^{-1}.

$$\tau_s = \frac{C_s}{R_h} \tag{1}$$

2.2 Breaking down the projected changes in soil carbon

From Equation 1, soil carbon (C_s) can be defined as shown by Equation 2. Future soil carbon stocks can be defined as initial soil carbon ($C_{s,0}$) plus a change in soil carbon (ΔC_s), as shown by Equation 3, where the subscript 0 denotes the initial state (historical simulation time-averaged between 1995-2005). Equation 3 can be expanded to give Equation 4, which can be simplified to give Equation 5.

$$C_s = R_h \tau_s \tag{2}$$

$$C_{s,0} + \Delta C_s = (R_{h,0} + \Delta R_h)(\tau_{s,0} + \Delta \tau_s) \tag{3}$$

$$C_{s,0} + \Delta C_s = R_{h,0}\tau_{s,0} + \tau_{s,0}\Delta R_h + R_{h,0}\Delta \tau_s + \Delta R_h \Delta \tau_s \tag{4}$$

$$\Delta C_s = \tau_{s,0}\Delta R_h + R_{h,0}\Delta \tau_s + \Delta R_h \Delta \tau_s \tag{5}$$

To isolate the above and below ground effects on soil carbon, the separate effects due to changes in NPP and changes due to τ_s are considered (Todd-Brown et al., 2014). For carbon to be conserved however, the difference between the global fluxes NPP and R_h in a transient climate must be taken into account, where the difference is defined as the Net Ecosystem Productivity (NEP), as shown in Equation 6.

$$\mathrm{NEP} = \mathrm{NPP} - \mathrm{R_h} \tag{6}$$

Equation 6 can be substituted into Equation 5, to obtain an equation for ΔC_s in terms of NPP, NEP and τ_s (Equation 7).

$$\Delta C_s = \tau_{s,0}\Delta(\mathrm{NPP} - \mathrm{NEP}) + (\mathrm{NPP}_0 - \mathrm{NEP}_0)\Delta\tau_\mathrm{s} + \Delta(\mathrm{NPP} - \mathrm{NEP})\Delta\tau_\mathrm{s} \quad (7)$$

If the initial state is a steady-state, the initial NEP (NEP_0) will be approximately equal to zero. However, as our initial state is defined as the end of the historical simulation, NEP_0 will therefore be non-zero as a result of the contemporary global land carbon sink. ESMs may also include additional carbon fluxes that cause changes to the resultant soil carbon inputs, such as: grazing, harvest, land-use change, and fire (Todd-Brown et al., 2014). The ΔNEP terms in Equation 7 implicitly includes these effects.

Finally, Equation 7 can be expanded to give Equation 8, and the individual responses which make up the total change in soil carbon (ΔC_s) can be broken-down into 6 components:

$$\Delta C_s = \tau_{s,0}\Delta\mathrm{NPP} - \tau_{s,0}\Delta\mathrm{NEP} + \mathrm{NPP}_0\Delta\tau_\mathrm{s} - \mathrm{NEP}_0\Delta\tau_\mathrm{s} + \Delta\mathrm{NPP}\Delta\tau_\mathrm{s} - \Delta\mathrm{NEP}\Delta\tau_\mathrm{s} \quad (8)$$

Equation 7 is exact for given time-varying values of NPP, NEP and τ_s~~, but in this form it does not cleanly separate into contributions due to changes in each of these factors. A linear approximation is therefore made (assuming $\Delta\mathrm{NPP}/\mathrm{NPP} << 1$ and $\Delta\tau_s/\tau_s << 1$), which allows for the cross-terms to be neglected ($\Delta\mathrm{NPP}\Delta\tau_\mathrm{s}$ and $\Delta\mathrm{NEP}\Delta\tau_\mathrm{s}$). The resultant~~ . The individual terms in Equation 8 are defined as given below.

$$\Delta C_{s,NPP} \approx \tau_{s,0}\Delta\mathrm{NPP} \quad (9)$$

$$\Delta C_{s,NEP} \approx -\tau_{s,0}\Delta\mathrm{NEP} \quad (10)$$

$$\Delta C_{s,\tau} \approx \mathrm{NPP}_0\Delta\tau_\mathrm{s} \quad (11)$$

$$\Delta C_{s,\tau_{NEP}} \approx -\mathrm{NEP}_0\Delta\tau_\mathrm{s} \quad (12)$$

Where, $\Delta C_{s,NPP}$ is the change in soil carbon due to changes in NPP, $\Delta C_{s,NEP}$ is the change in soil carbon due to changes in NEP, and $\Delta C_{s,\tau}$ is the change in soil carbon due to changes in τ_s (with $\Delta C_{s,\tau_{NEP}}$ accounting for non-equilibrium). The two additional terms are: the non-linear term between NPP and τ_s ($\Delta\mathrm{NPP}\Delta\tau_\mathrm{s}$) and the non-linear term between NEP and τ_s ($\Delta\mathrm{NEP}\Delta\tau_\mathrm{s}$).

3 Results and Discussion

3.1 Projected changes in soil carbon

A reduced spread in projected end of 21st century estimates of ΔC_s is seen in CMIP6 compared to CMIP5 (Fig. 1). This reduced spread is shown in Fig. 1, where projections of ΔC_s by 2100 in CMIP6 are compared with those from CMIP5 across the different future scenarios. The reduced range of projected changes is seen across all future scenarios (*SSP126* and *RCP2.6*, *SSP245* and *RCP4.5*, *SSP585* and *RCP8.5*), with the range in CMIP6 consistently less than 50% of the equivalent range in CMIP5 (Fig. 1). This reduced spread in projections is also suggested by a reduced standard deviation about the ensemble mean ΔC_s in CMIP6 compared with CMIP5, which is consistently reduced by 50% across all future climate scenarios (Tables 2 and A1, bottom rows). It is noted that the large range in CMIP5 estimates is mostly a result of large increases in C_s in HadGEM2-ES and MPI-ESM-LR, together with the large C_s losses in GISS-E2-R (Fig. 1). An updated CMIP6 version of the GISS-E2-R model is not included in this analysis of this study, which could contribute to the reduced uncertainty from CMIP5. However, the updated equivalent CMIP6 models UKESM1-0-LL (from HadGEM2-ES) and MPI-ESM1-2-LR (from MPI-ESM-LR) have projected estimates of ΔC_s which are more consistent with the other models in the CMIP6 ensemble.

Nearly all of the ESM projections in CMIP6 suggest an increase in C_s by 2100, however CMIP5 models project both increases (positive ΔC_s) and decreases (negative ΔC_s) in soil carbon during the 21st century (Fig. 1). In CMIP5 projections, the future responses of soil carbon range from an increase of 23.2% (HadGEM2-ES) to a decrease of 6.50% (GISS-E2-R) in *RCP8.5*, where across all future scenarios approximately half of the models show increases and half show decreases in ΔC_s (Table A1). In CMIP6, the future responses of soil carbon range from an increase of 12.5% (MPI-ESM1-2-LR) to a decrease of 2.25% (ACCESS-ESM1.5) in *SSP585*, however the majority of models predict an increase in ΔC_s across all future scenarios (Table 2).

Despite more consistent projections of increased ΔC_s in CMIP6 compared with CMIP5, it is apparent that greater CO_2 forcing (i.e. *SSP585* compared with *SSP126*) does not always imply a greater magnitude of increased C_s. By contrast to what is seen in CMIP6, the majority of CMIP5 models project an increased magnitude in estimated ΔC_s with increased CO_2 forcing (Fig. 1). In CMIP6, half the models (CESM2, CNRM-ESM2-1, IPSL-CM6A-LR, NorESM2-LM, and UKESM1-0-LL) estimate less soil carbon accumulation by 2100 (i.e. a smaller increase or a greater decrease) in *SSP585* when compared with *SSP126*. This effect is most prominent in BCC-CSM2-MR and UKESM1-0-LL, where a turning point from increasing to decreasing soil carbon is seen in the mid-century of the *SSP585* projections (Fig. 2). This is opposed to an estimated increase in soil carbon storage with increased forcing, which is generally seen in CMIP5 and the remaining CMIP6 models (CanESM5, MIROC-ES2L, and MPI-ESM1-2-LR). This finding is likely due to a saturation of the CO_2 fertilisation effect, compared with no saturation of increased respiration with warming in these ESMs. This finding suggests a potential limit to ΔC_s increase and a reduced likelihood of a carbon sink under more extreme levels of climate change.

The spatial pattern of estimated ΔC_s (Fig. 3) is quite variable between CMIP6 ESMs. For example in the tropical regions, where increases in soil carbon can be seen in 6 of the CMIP6 ESMs (BCC-CSM2-MR, CanESM5, CESM2, MIROC-ES2L, and NorESM2-LM), but decreases are seen in the remaining 4 (ACCESS-ESM1-5, CNRM-ESM2-1, IPSL-CM6A-LR, and

UKESM1-0-LL). There is a lack of agreement in the high northern latitudes amongst the CMIP6 ESMs (Fig. 3), where it is known that the uncertainty surrounding the fate of soil carbon stocks in these regions is particularly important due to the large magnitude of carbon stored (Burke et al., 2020; Jackson et al., 2017). It has previously been found that a high accumulation of northern latitude C_s is predicted amongst CMIP5 ESMs, however this C_s response has not been suggested in empirical studies (Todd-Brown et al., 2014). The results here suggest that this accumulation (increased ΔC_s) remains in the majority of CMIP6 ESMs (Fig. 3), although reductions in northern latitude soil carbon stocks were found in 3 CMIP6 ESMs (BCC-CSM2-MR, CESM2 and NorESM2-LM, with BCC-CSM2-MR seeing reductions in a greater area). These ESMs which predicted northern latitude C_s reductions were previously found to simulate historical northern latitude soil carbon stocks which are more consistent with the observational estimates seen in these regions (Varney et al., 2022).

3.2 Future changes to land-atmosphere fluxes

The projected ΔC_s is a result of the changing input and output land-atmosphere fluxes under climate change. To a first order, the response of soil carbon will be determined by changes to NPP and to τ_s (see Equation 7). In this section, future projections of these fluxes are analysed in both CMIP6 and CMIP5 ESMs.

3.2.1 Net Primary Productivity

NPP is projected by CMIP6 ESMs to increase during the 21$^{\text{st}}$ century, with a greater increase with increasing climate forcing (across SSP scenarios). This result is consistent with the projections of ΔNPP amongst the CMIP5 models (Fig. 4; Todd-Brown et al. (2014)). Projections amongst ESMs however, show disagreement in the magnitude of ΔNPP by 2100 across all future climate scenarios, where a projected CMIP6 ensemble increase of 24.6 $\pm$ 16.9 PgC yr^{-1} is seen in *SSP585*. The largest projections of ΔNPP amongst the CMIP6 models are seen in CanESM5 and BCC-CSM2-MR, where increases of 65.8 PgC yr^{-1} (47% increase) and 39.4 PgC yr^{-1} (43% increase) are projected by 2100 under *SSP585*, respectively. This is compared to ACCESS-ESM1-5 which has the lowest projected changes amongst the CMIP6 models with an increase of only 4.07 PgC yr^{-1} (10% increase) by 2100 under *SSP585* (Table 3).

The CMIP6 ensemble sees a slightly increased range in end of century ΔNPP compared with CMIP5, across all future scenarios (Tables 3 and A2). Fig. 4 suggests that the increased range is mostly due to outlying projections of ΔNPP (CanESM5), where greater increases are seen compared to the majority of models within the ensemble. It is noted that a cluster of ESMs which have similar projections of ΔNPP is seen within CMIP6 (CESM2, MIROC-ES2L, MPI-ESM1-2-LR, NorESM2-LM, and UKESM1-0-LL). The cluster is found to be made up of ESMs which include the simulation of an interactive nitrogen cycle (shown by the dashed lines throughout this study), which is a common addition within CMIP6 ESMs (ACCESS-ESM1.5, CESM2, MIROC-ES2L, MPI-ESM1-2-LR, NorESM2-LM and UKESM1-0-LL; Davies-Barnard et al. (2020)). ACCESS-ESM1-5 is the only model which simulates interactive nitrogen and does not predict consistent ΔNPP with the other nitrogen ESMs in CMIP6, however the projections of ΔNPP in ACCESS-ESM1-5 is consistent with the projections of NorESM1-M in CMIP5, which is the only CMIP5 model considered here to simulate interactive nitrogen (~~Fig. 4~~Table 1).

3.2.2 Soil carbon turnover time

Future τ_s is projected by CMIP6 ESMs to decrease by 2100 across all future SSP scenarios (Fig. 5). A greater reduction in τ_s is seen with increased climate forcing scenario, where a reduced τ_s is a faster soil carbon turnover time, and implies that carbon is cycled back to the atmosphere in less time due to an increased carbon output from the soil (increased R_h, see Equation 1). This result is consistent with the projections of $\Delta\tau_s$ amongst the CMIP5 models (Fig. 5; Todd-Brown et al. (2014)). However, it is found that greater variation exists amongst the CMIP6 ESMs end of century estimates, where a projected CMIP6 ensemble $\Delta\tau_s$ value of -7.65 $\pm$ 5.65 years is seen in *SSP585* compared to -6.13 $\pm$ 3.03 years for CMIP5 ESMs in *RCP8.5* (Tables 3 and A2).

The CMIP6 ESMs with the greatest reductions in effective global τ_s by 2100 is seen in BCC-CSM2-MR, CESM2 and NorESM2-LM, where global carbon turnover in the soil is at least 14 years faster at the end of the *SSP585* simulation compared to the start of the 21$^{\mathrm{st}}$ century (historical reference). The CMIP6 models with the least change in effective global τ_s are ACCESS-ESM1-5, IPSL-CM6A-LR, and MPI-ESM1-2-LR, where global carbon turnover in the soil is only around 2 years faster at the end of the *SSP585* simulation (Table 3). The increased range in CMIP6 from CMIP5 is primarily due to the large τ_s reductions seen in the CMIP6 models NorESM2-LM, CESM2 and BCC-CSM2-MR (Fig. 5).

3.3 Breaking down the projected changes in soil carbon

To understand the projected end of century changes in soil carbon storage (ΔC_s) in ESMs, the individual responses of soil carbon due to changes in NPP ($\Delta C_{s,NPP}$, see Equation 9) and the response due to changes in τ_s ($\Delta C_{s,\tau}$, see Equation 12) were diagnosed for both CMIP5 and CMIP6 as shown in Fig. 6. Future ΔC_s (blue bars) is found to mostly a result of the net effect of the linear terms: $\Delta C_{s,NPP}$ (dark green bars) and $\Delta C_{s,\tau}$ (red bars). However, there are also non-negligible contributions from the non-linear term: $\Delta\mathrm{NPP}\Delta\tau_\mathrm{s}$ (black bars), and a small addition due to the non-equilibrium terms: $\Delta C_{s,NEP}$ (light green bars), $\Delta C_{s,\tau_{NEP}}$ (pink bars), and $\Delta\mathrm{NEP}\Delta\tau_\mathrm{s}$ (grey bars).

The importance of investigating the individual processes which contribute to the net ΔC_s in ESMs can be seen (Fig. 6). In Fig. 6 it is seen that the net ΔC_s is relatively small compared to the individual changes from the derived components, where especially large magnitudes are seen in the increased C_s due to increased ΔNPP ($\Delta C_{s,NPP}$) and the decreased C_s due to reduced $\Delta\tau_s$ ($\Delta C_{s,\tau}$). For example, in *SSP585* there is a range of approximately 170 PgC in net ΔC_s, from an increase of 132 PgC (CNRM-ESM2-1) to a reduction of 35 PgC (BCC-CSM2-MR). However, the $\Delta C_{s,NPP}$ contribution has a much larger range of 1442 PgC, from an increase of 95 PgC (ACCESS-ESM1-5) to an increase of 1517 PgC (NorESM2-LM). Similarly, $\Delta C_{s,\tau}$ has a range of 756 PgC, from a decrease of 115 PgC (ACCESS-ESM1-5) to a decrease of 871 PgC (NorESM2-LM).

The magnitude of change seen from the individual feedbacks ($\Delta C_{s,NPP}$ and $\Delta C_{s,\tau}$) is not obviously related to the resultant magnitude of soil carbon change (Fig. A1). For example, NorESM2-LM projects large $\Delta C_{s,NPP}$ and $\Delta C_{s,\tau}$ values (1517 PgC and -871 PgC in *SSP585*, respectively), however a relatively small net change in soil carbon (49 PgC in *SSP585*). Conversely, CNRM-ESM2-1 projects smaller $\Delta C_{s,NPP}$ and $\Delta C_{s,\tau}$ values (667 PgC and -413 PgC in *SSP585*, respectively), but a larger net soil carbon change (132 PgC in *SSP585*). Within ESMs, it is found that the change in soil carbon is determined by the

relationship between all the contributing terms to the net ΔC_s response, as opposed to the absolute size of a given contribution (Fig. 6).

Surprisingly, a very strong correlation is found amongst the ESMs in CMIP6 (r^2 value of 0.97) between the linear terms $\Delta C_{s,NPP}$ and $\Delta C_{s,\tau}$ (Fig. 7(a)). This leads to the partially cancelling of the terms, with a resultant relatively small net ΔC_s. When comparing with the CMIP5 ensemble, a lower correlation between $\Delta C_{s,NPP}$ and $\Delta C_{s,\tau}$ is seen (r^2 value of 0.084, Fig. 7(a)). This correlation amongst CMIP6 ESMs results in net ΔC_s being more clustered in CMIP6 compared to CMIP5 (Fig. 1), despite a similarly large variation in the individual contributions (Fig. 6). The strong CMIP6 correlation ($r^2 = 0.97$) remains when the fractional changes ($\Delta C_{s,NPP}/C_{s,0}$ and $\Delta C_{s,\tau_{NPP}}/C_{s,0}$, where $C_{s,0}$ is initial soil carbon stocks) are plotted instead (Fig. 7(b)).

Fig. 6 also shows that the differences in ESM projections of ΔC_s are partly due to differing magnitudes of the non-linear term ($\Delta\mathrm{NPP}\Delta\tau_\mathrm{s}$). ~~The non-linear $\Delta\mathrm{NPP}\Delta\tau_\mathrm{s}$ term having non-negligible contributions to future ΔC_s means the initial~~ A linear assumption is commonly used which would allow these cross-terms to be neglected ($\Delta\mathrm{NPP}/\mathrm{NPP} << 1$ and $\Delta\tau_s/\tau_s << 1$~~assumptions were not valid in this case. The~~ ; Koven et al. (2015)). However, the ESM projected magnitudes of $\Delta\mathrm{NPP}\Delta\tau_\mathrm{s}$ are found to be relatively large, especially in the more extreme climate scenarios (Fig. 6). In *SSP585*, a range from a decreased C_s of 11 PgC (ACCESS-ESM1-5) to a decreased C_s of 599 PgC (BCC-CSM2-MR) is found amongst the CMIP6 models due to only the $\Delta\mathrm{NPP}\Delta\tau_\mathrm{s}$ term, and in some cases values greater magnitudes are seen than the net ΔC_s (BCC-CSM2-MR, CanESM5, CESM2, NorESM2-LM, and UKESM1-0-LL). The term is greater when there are large and counteracting magnitudes of $\Delta\mathrm{NPP}$ and $\Delta\tau_s$, which results in a non-negligible product.

Additionally, to obtain the overall change in soil carbon seen in the models, contributions from the non-equilibrium terms ($\Delta C_{s,NEP}$, $\Delta C_{s,\tau_{NEP}}$, and $\Delta\mathrm{NEP}\Delta\tau_\mathrm{s}$) must also be included (Fig. 6). The $\Delta C_{s,NEP}$ term represents the change in soil carbon due to the net carbon sink during the 21$^{\mathrm{st}}$ century, which exists while the climate is in a transient state due to continuous climate change. By definition, the magnitude of $\Delta C_{s,NEP}$ is negative if ΔNEP is positive, which implies a greatest or faster increase in NPP with respect to R_h seen in the majority of ESMs. The contribution from these terms is found to be relatively small in most models, but not in all. In *SSP585*, projections of $\Delta C_{s,NEP}$ amongst CMIP6 models range from a reduction of 333 PgC (NorESM2-LM) to a gain of 8.74 PgC (ACCESS-ESM1-5). In CMIP5, exceptions where greater $\Delta C_{s,NEP}$ terms are found in the GISS-E2-R and MPI-ESM-LR models, implying the models are far from equilibrium at the end of the 21$^{\mathrm{st}}$ century. The change in soil carbon due to the change in NEP ($\Delta C_{s,NEP}$) is often found to be greater in the models which see greater magnitudes of $\Delta C_{s,NPP}$ and $\Delta C_{s,\tau}$.

3.4 Investigating the emergent relationship between $\Delta C_{s,NPP}$ and $\Delta C_{s,\tau}$

In this subsection, the emergent relationship between $\Delta C_{s,NPP}$ and $\Delta C_{s,\tau}$ present across the CMIP6 ensemble is ~~further~~ investigated using the idealised C4MIP simulations (see Methods). This enables investigation of the negative correlation without additional complex processes which are included in the SSP simulations. By isolating the sensitivities to CO_2 and climate, we can more easily identify the processes which results in the apparent coupling between NPP and soil carbon turnover time in CMIP6 ESMs. Fig. 8 presents the relationship between $\Delta C_{s,NPP}$ and $\Delta C_{s,\tau}$ for each CMIP6 ESMs as in Fig. 7, but for

the *full* 1% CO_2, *BGC* (CO_2 only), and *RAD* (climate only) simulations. It is found that $\Delta C_{s,NPP}$ and $\Delta C_{s,\tau}$ are strongly correlated in the *full* 1% CO_2 simulation, at both 2xCO_2 (r^2 value of 0.925) and 4xCO_2 (r^2 value of 0.839). The correlation is found to remain in the *BGC* simulation, where r^2 values are found to be 0.838 and 0.708 for 2xCO_2 and 4xCO_2, respectively. ~~The slightly reduced correlation in the *BGC* simulation at 4xCO_2 suggests a potential limit to the effect at high levels of atmospheric CO_2.~~ A correlation is also seen in the *RAD* simulation at 2xCO_2 (r^2 value of 0.601), however the correlation in the *RAD* simulation does not hold at 4xCO_2, where the r^2 value reduces to 0.265. The reduced correlation in the *RAD* simulation at 4xCO_2 suggests a reduced relationship between NPP and τ_s at the more extreme temperature changes that are projected at high levels of atmospheric CO_2 (without the direct effects of CO_2 in this run).

For each CMIP6 ESM, NPP and τ_s are found to be strongly inversely correlated in the *full* 1% CO_2 simulation (Fig. 9). The r^2 values between $\mathrm{NPP}/\mathrm{NPP}_0$ and $\tau_{s,0}/\tau_s$ (where the subscript 0 denotes the historical state) are found to be greater than 0.95 in all models except for ACCESS-ESM1-5 (where an r^2 value of 0.65 is found due to a breakdown at high CO_2 levels). In the *BGC* simulation, a similar relationship between $\mathrm{NPP}/\mathrm{NPP}_0$ and $\tau_{s,0}/\tau_s$ is seen up until approximately 2xCO_2 in all ESMs (approximately 50% of the simulation). However, how the relationship between $\mathrm{NPP}/\mathrm{NPP}_0$ and $\tau_{s,0}/\tau_s$ changes throughout the *BGC* simulation (between 2xCO_2 and 4xCO_2) varies between models. A greater rate of $\mathrm{NPP}/\mathrm{NPP}_0$ increase compared to $\tau_{s,0}/\tau_s$ is seen at greater levels of climate forcing for the majority of CMIP6 ESMs (BCC-CSM2-MR, CanESM5, GFDL-ESM4, IPSL-CM6A-LR, MIROC-ES2L, MPI-ESM1-2-LR and UKESM1-0-LL), where the τ_s changes appear to saturate and a limit to the increase is seen. In these ESMs, the changes seen in the *full* and *BGC* simulations differ due to a climate effect (shown by the *RAD* simulation), which appears to negate the apparent limit or saturation seen in the $\tau_{s,0}/\tau_s$ increase in the *BGC* simulation (Fig. 9). In CESM2 and NorESM2-LM (containing the same land surface model component), a consistent relationship is seen in both the *full* 1% CO_2 and *BGC* simulations, suggesting the changes in NPP and τ_s are primarily ~~due to~~ driven by changes in CO_2 concentrations ~~,~~or that the climate affects cancel out to a resultant net zero change. In ACCESS-ESM1-5, a consistent relationship is seen in the *full* 1% CO_2, *BGC* and *RAD* simulations, suggesting a greater sensitivity of NPP to environmental climate changes compared to the other CMIP6 ESMs (Fig. 9).

It has been shown in this subsection that the correlation between $\Delta C_{s,NPP}$ and $\Delta C_{s,\tau}$, as seen in the SSP simulations (Fig. 7 and Fig. 8), is also evident in the *full* 1% CO_2 C4MIP simulation. This suggests the relationship is not a result of additional processes included in the SSP simulations compared to the C4MIP experiments, such as land use change (Jones et al., 2016). An additional explanation for the coupling could be similarities in the modelled sensitivities of NPP and R_h to changes in climate. For example, if NPP and soil respiration rate both increased with warming, a negative correlation between $\Delta C_{s,NPP}$ and $\Delta C_{s,\tau}$ would be seen. However, under these circumstances the negative correlation would not be seen in the CO_2 only runs (*BGC* simulation), as there is no global warming in these simulations (see Methods). Instead, a reduction in effective soil carbon turnover time is seen in the CO_2 only runs (*BGC* simulation; Fig. A2), which implies a non-climate response in τ_s and results in a NPP-τ_s negative correlation under changing atmospheric CO_2 alone (Fig. 9). Fig. 10 shows that the change in the effective soil carbon turnover time in the CO_2 only simulation (*BGC* simulation) accounts for at least 50% of the total change in the effective soil carbon turnover time in the *full* 1% simulation across CMIP6 ESMs.

3.5 The role of false priming

Koven et al. (2015) presents the concept of ~~'false priming'~~false priming, which describes a reduction in effective ~~carbon turnover~~ soil carbon turnover time (τ_s) due to increases in productivity (NPP). It was defined as ~~false priming~~ 'false priming' due to the impact being similar to the 'true priming' process, but occurs without simulating the priming mechanisms; where priming is defined as the stimulation of decomposition of soil carbon (reducing τ_s) due to input of carbon to the soil (Liu et al., 2020). The false priming reduction in effective τ_s is a transient phenomenon that arises in soil models that represent multiple carbon pools with different turnover times. Under continually increasing NPP, proportionally more of the additional input litter carbon is put into the faster soil carbon pools than the slow, which brings down the global average effective τ_s value of the soil.

In this subsection, false priming is explored as a possible explanation for the ~~correlations~~ negative correlation seen between NPP ~~changes~~ and τ_s~~changes~~, which are seen even in the *BGC* simulations (CO_2 only) where the climate does not change significantly (~~second row of Fig. 8).~~ Fig. 10).

Koven et al. (2015) demonstrates false priming with a simple three-box soil carbon model, which has been adapted here to use notation consistent with the rest of this study:

$$\frac{dC_{s,1}}{dt} = NPP - \frac{C_{s,1}}{\tau_{s,1}} \tag{13}$$

$$\frac{dC_{s,2}}{dt} = \frac{e_1 C_{s,1}}{\tau_{s,1}} - \frac{C_{s,2}}{\tau_{s,2}} \tag{14}$$

$$\frac{dC_{s,3}}{dt} = \frac{e_2 C_{s,2}}{\tau_{s,2}} - \frac{C_{s,3}}{\tau_{s,3}} \tag{15}$$

$$R_h = \frac{(1-e_1)C_{s,1}}{\tau_{s,1}} + \frac{(1-e_2)C_{s,2}}{\tau_{s,2}} + \frac{(1-e_3)C_{s,3}}{\tau_{s,3}} \tag{16}$$

$$C_s = C_{s,1} + C_{s,2} + C_{s,3} \tag{17}$$

$$\tau_{s,1} = 1, \tau_{s,2} = 10, \tau_{s,3} = 100, e_1 = 0.3, e_2 = 0.3, e_3 = 0. \tag{18}$$

where, $C_{s,1}$, $C_{s,2}$, $C_{s,3}$ represent the carbon stored in soil carbon pools 1, 2, and 3 and make up the total soil carbon (C_s). Similarly, $\tau_{s,i}$ are the respective soil carbon turnover times, which are given defined values of increasing turnover times in years: fast (1 year), medium (10 years) and slow (100 years). NPP represents the carbon input into the system, where carbon is inputted into pool 1 ($C_{s,1}$), then flows to pool 2 ($C_{s,2}$) and then 3 ($C_{s,3}$). The coefficients e_i represents the fraction of carbon that is passed to the next pool rather than outputted as heterotrophic respiration (R_h).

At equilibrium, the change in the soil carbon pools will be zero ($dC_{s,i}/dt = 0$), so the amount of soil carbon present within each pool depends on the input carbon and turnover time of the pool ($\tau_{s,i}$). Under increasing NPP, the three-box model can

be used to investigate the subsequent changes to soil carbon in the 3 carbon pools ($C_{s,1}$, $C_{s,2}$, $C_{s,3}$) based on changing input alone, due to each pool having a fixed $\tau_{s,i}$ value. This removes the $\Delta\tau_s$ from changing environmental and microbial conditions (Koven et al., 2015; Wieder et al., 2015a; Exbrayat et al., 2013). The effective τ_s is calculated by definition, using Equation 1.

Fig. 11(a) produces a simulation of the response of this three-box model to an NPP input flux that increases at 0.3% per year, and where the soil carbon boxes are initialised at 0 (reproducing Fig. 12 in Koven et al. (2015)). The ~~false priming decline in~~ greater fraction of ΔC_s in the fast soil carbon pool compared to the slow can be seen, which results in a decline in the effective τ_s of the system. This decline in effective τ_s with increasing NPP is clear ~~, and for this set of parameters offsets about 40% of the increase in soil carbon that would arise from the NPP increase alone.~~ and demonstrates false priming (Fig. 11(a)). Fig. 11(b) again demonstrates that false priming is a transient effect associated with ~~a disequilibrium in~~ the distribution of soil carbon between the 3 pools, which emerges from the differences in the mass-weighted and flux-weighted responses. It shows results from the same model, but for a step increase in global NPP from 50 PgC yr^{-1} to 70 PgC yr^{-1} at year 100. The fast soil carbon pool reaches equilibrium before the slower soil carbon pool resulting in the instantaneous decline in τ_s of about 10%, which eventually reduces to return the soil to the original τ_s~~, but this~~ . However, this transient effect occurs on the timescale of the slowest carbon pool and so may take many centuries.

The same three-box model can also be used to investigate the relationship between the contributions of changes in NPP ($\Delta C_{s,NPP}$) and τ_s ($\Delta C_{s,\tau}$) to net soil carbon change that was noted in both Fig. 7 and Fig. 8. Fig. 12 plots $\Delta C_{s,NPP}$ against $\Delta C_{s,\tau}$ from the three-box model after 70 years of runs that assume different rates of increase of NPP (0% to 0.8% per year in increments of 0.05%). A clear relationship between $\Delta C_{s,NPP}$ and $\Delta C_{s,\tau}$ is seen, with greater false priming (more negative $\Delta C_{s,\tau}$) when the NPP increase is larger (more positive $\Delta C_{s,NPP}$). The similarity of Fig. 12 to both Fig. 7 and Fig. 8 is clear, suggesting that false priming and the structure of the soil carbon models within the ESMs is likely contributing to these correlations in CMIP6 (and to a lesser extent in CMIP5)~~are predominantly due to false priming~~.

It is noted that the influence of false priming was stronger in the *full* 1% CO_2 and *BGC* (CO_2 only) simulations, compared to the *RAD* (climate only) simulation ~~.~~(Fig. 8). This is likely due to the *RAD* simulation not seeing sufficient NPP change, and therefore sufficient input of soil carbon, for the false priming ~~affect~~ effect to be significant (see Fig. A2)~~, opposed to false priming being a direct result of atmospheric CO_2 change~~. Additionally, the direct effect of temperature changes on τ_s in the *RAD* simulation (in the absence of atmospheric CO_2 changes) is likely to dampen the correlation to NPP changes, due to both direct and indirect $\Delta\tau_s$ influences in this case (Varney et al., 2020). False priming is dependent on the structure of the soil carbon model within the ESM. The reduced effective soil carbon turnover time occurring in a transient system, without any external sensitivities on τ_s, is a consequence of varying turnover times between different soil carbon pools.

This study has highlighted how false priming has contributed to a reduced spread in ΔC_s ESM projections in CMIP6, due to a cancellation effect seen between increases due to ΔNPP ($\Delta C_{s,NPP}$) and decreases due to $\Delta\tau_s$ ($\Delta C_{s,\tau}$). The extent of false priming within ESM projections will depend on the distribution of carbon within soil carbon pools and how litter carbon is allocated between pools with fast and slow turnover times (Koven et al., 2015). Fig. 10(c) shows the fraction of $\Delta\tau_s$ due to ΔCO_2, which can be used as a proxy to estimate the contribution of false priming to the overall projected $\Delta\tau_s$ in CMIP6 ESMs, which varies between approximately 50% (CanESM5 and MIROC-ES2L) to 90% (CESM2 and NorESM2-LM). A more

apparent false priming affect within CMIP6 could suggest an improved representation of the slower components of soil carbon since CMIP5, commonly by including more dead carbon pools within the ESM (Table 1). Based on observational radiocarbon estimates it has been found that CMIP5 ESMs underestimate carbon age within the soil (He et al., 2016; Shi et al., 2020), suggesting that ESMs underestimate the amount of carbon in the slow carbon pools. It has been shown that representing soil carbon ages more in line with radiocarbon estimates leads to a reduced potential for soil carbon sequestration in the future (He et al., 2016), which agrees qualitatively with the projected 21st century soil carbon changes as predicted by CMIP6 compared to CMIP5 found in this study.

On top of the role of false priming, additional factors within ESMs influence the magnitude of predicted ΔC_s. Generationally related ESMs between CMIP5 and CMIP6 allow us to highlight some key changes between the CMIP generations and to suggest potential model developments which may have contributed to the projected differences in future C_s. For example, within CMIP5 the models HadGEM2-ES and MPI-ESM-LR predicted the greatest increases in soil carbon within the ensemble, however within CMIP6 the updated versions UKESM1-0-LL and MPI-ESM1-2-LR predict reduced increases (Fig. 1). Both updated variants of these ESMs include the representation of interactive nitrogen in CMIP6 simulations (Table 1), which could limit carbon sequestration through limiting the magnitude of CO_2 fertilisation. Depending on the ratio of carbon to nitrogen within the soil however, accelerated decomposition due to soil warming can increase nitrogen mineralisation and alleviate the nutrient limitation in plants (Wiltshire et al., 2021; Todd-Brown et al., 2014). Additionally, MPI-ESM1-2-LR (CMIP6) sees an increased number of dead (soil) carbon pools compared with MPI-ESM-LR (CMIP5), whereas UKESM1-0-LL (CMIP6) from HadGEM2-ES (CMIP5) sees no change in the number of carbon pools. The increased number of dead carbon pools could contribute to the decrease in ΔC_s by either: a transient reduction due to false priming, or longer soil carbon turnover times resulting in carbon being stored in slower pools within the soil. It is noted that an investigation into the role of soil carbon pools in future soil carbon projections will require projections and allocation of C_s in individual soil pools within ESMs, which is beyond the scope of this study (Koven et al., 2015).

4 Conclusions

In this study, future projections of soil carbon change (ΔC_s) have been analysed using ESM output from the latest CMIP6 ensemble and were investigated under differing levels of climate change (future scenarios *SSP126*, *SSP245* and *SSP585*). The future projections made by CMIP6 ESMs were also compared against equivalent projections made by the previous generation of ESMs in the CMIP5 ensemble (future scenarios *RCP2.6*, *RCP4.5* and *RCP8.5*) to investigate whether recent model improvements have reduced the uncertainty surrounding the future soil carbon response. Additionally, ΔC_s was broken down into the individual components which contribute to the net change within ESMs, with a specific focus on increases due to increases in NPP ($\Delta C_{s,NPP}$) and decreases due to reductions in turnover ($\Delta C_{s,\tau}$). Below the key conclusions from this study are listed:

1. An apparent reduction in uncertainty of end of 21st century ΔC_s projections is suggested in CMIP6 compared to CMIP5.

2. However, the same reduction in projection uncertainty is not suggested surrounding the soil carbon controls: Net Primary Productivity (NPP) and the effective soil carbon turnover time ($\tau_s = C_s/R_h$), and the subsequent effects on future soil carbon storage ($\Delta C_{s,NPP}$ and $\Delta C_{s,\tau}$, respectively).

3. ~~It is noted that the results in this study suggest the inclusion of a interactive nitrogen cycle within simulations constrains the future responses to NPP and shows progress in CMIP6 models.~~

4. The derived linear terms which contribute to net soil carbon change, the response of soil carbon due to changes in NPP ($\Delta C_{s,NPP}$) and the response due to changes in τ_s ($\Delta C_{s,\tau}$), are found to have a strong relationship in CMIP6, with a more significant correlation than what was seen in CMIP5. This correlation is likely to be a cause of the reduction in the ΔC_s projection spread across the CMIP6 ensemble.

5. ~~The~~ False priming was found to likely be contributing to the apparent emergent relationship between $\Delta C_{s,NPP}$ and $\Delta C_{s,\tau}$ in CMIP6 ESMs~~was found to be a result of false priming~~, which describes a transient ~~increase in effective~~ reduction in effective soil carbon turnover time due to increased input of carbon to the soil. The net effect of false priming is a coupling affect between ΔNPP and $\Delta\tau_s$ ~~,~~and results in a reduced range of future ΔC_s predictions in CMIP6.

6. ~~It is recommended that the full extent of false priming on future soil carbon is understood, where if increased carbon inputs to soil carbon pools preferentially enters fast soil carbon pools, this could limit the maximum increase in soil carbon storage in the future~~Our study highlights the significant role that false priming can play under transient changes in atmospheric CO_2 and climate. We advise caution in the interpretation of changes in the effective soil carbon turnover time in terms of climate affects alone. Idealised C4MIP simulations, which can be used to separate the effects of CO_2 and climate on the effective soil carbon turnover time, are very useful to assess the role of false priming in models. Understanding these factors will be key to predicting soil carbon changes over the next 100 years.

Understanding and quantifying soil carbon feedbacks under anthropogenic emissions of CO_2 is critical for calculating an accurate global carbon budget, which is required if Paris Agreement targets are to be met (Friedlingstein et al., 2022). This study highlights the importance of considering the individual soil driven carbon feedbacks under climate change when determining the overall response of global soil carbon storage, and suggests the need for constraints on the magnitudes of these feedbacks in CMIP6 to reduce uncertainty in projections of future land carbon storage.

Code availability. Code is available on GitHub (https://github.com/rebeccamayvarney/CMIP6_dCs).

Data availability. The CMIP data analysed during this study are available online: CMIP6 (https://esgf-node.llnl.gov/search/cmip6/) and CMIP5 (https://esgf-node.llnl.gov/search/cmip5/).

Author contributions. RMV, SEC and PMC outlined the study. RMV completed the analysis and produced the figures. All the co-authors provided guidance on the study at various times and suggested edits to the draft manuscript.

Competing interests. The authors have declared no competing interests.

Acknowledgements. This research has been supported by the European Research Council, Emergent Constraints on Climate–Land feedbacks in the Earth System project (ECCLES; grant no. 742472) and Climate–Carbon Interactions in the Current Century project (4C; grant no. 821003) (RMV and PMC). SEC was supported by a Natural Environment Research Council independent research fellowship (grant no. NE/R015791/1). AJW and EJB were supported by the Joint UK BEIS/Defra Met Office Hadley Centre Climate Programme (grant no. GA01101). We thank the World Climate Research Programme's Working Group on Coupled Modelling and the climate modelling groups for producing and making their model output available.

References

Arora, V. and Boer, G.: Uncertainties in the 20th century carbon budget associated with land use change, Global Change Biology, 16, 3327–3348, 2010.

Arora, V., Boer, G., Christian, J., Curry, C., Denman, K., Zahariev, K., Flato, G., Scinocca, J., Merryfield, W., and Lee, W.: The effect of terrestrial photosynthesis down regulation on the twentieth-century carbon budget simulated with the CCCma Earth System Model, Journal of Climate, 22, 6066–6088, 2009.

Arora, V. K., Boer, G. J., Friedlingstein, P., Eby, M., Jones, C. D., Christian, J. R., Bonan, G., Bopp, L., Brovkin, V., Cadule, P., et al.: Carbon–concentration and carbon–climate feedbacks in CMIP5 Earth system models, Journal of Climate, 26, 5289–5314, 2013.

Arora, V. K., Katavouta, A., Williams, R. G., Jones, C. D., Brovkin, V., Friedlingstein, P., Schwinger, J., Bopp, L., Boucher, O., Cadule, P., et al.: Carbon–concentration and carbon–climate feedbacks in CMIP6 models and their comparison to CMIP5 models, Biogeosciences, 17, 4173–4222, 2020.

Bentsen, M., Bethke, I., Debernard, J. B., Iversen, T., Kirkevåg, A., Seland, Ø., Drange, H., Roelandt, C., Seierstad, I. A., Hoose, C., et al.: The Norwegian Earth System Model, NorESM1-M–Part 1: description and basic evaluation of the physical climate, Geoscientific Model Development, 6, 687–720, 2013.

Best, M., Pryor, M., Clark, D., Rooney, G., Essery, R., Ménard, C., Edwards, J., Hendry, M., Porson, A., Gedney, N., et al.: The Joint UK Land Environment Simulator (JULES), model description–Part 1: energy and water fluxes, Geoscientific Model Development, 4, 677–699, 2011.

Boucher, O., Servonnat, J., Albright, A. L., Aumont, O., Balkanski, Y., Bastrikov, V., Bekki, S., Bonnet, R., Bony, S., Bopp, L., et al.: Presentation and evaluation of the IPSL-CM6A-LR climate model, Journal of Advances in Modeling Earth Systems, 12, e2019MS002 010, 2020.

Burke, E. J., Ekici, A., Huang, Y., Chadburn, S. E., Huntingford, C., Ciais, P., Friedlingstein, P., Peng, S., and Krinner, G.: Quantifying uncertainties of permafrost carbon–climate feedbacks, Biogeosciences, 14, 3051–3066, 2017.

Burke, E. J., Zhang, Y., and Krinner, G.: Evaluating permafrost physics in the Coupled Model Intercomparison Project 6 (CMIP6) models and their sensitivity to climate change, The Cryosphere, 14, 3155–3174, 2020.

Canadell, J., Monteiro, P., Costa, M., Cotrim da Cunha, L., Cox, P., Eliseev, A., Henson, S., Ishii, M., Jaccard, S., Koven, C., Lohila, A., Patra, P., Piao, S., Rogelj, J., Syampungani, S., Zaehle, S., and Zickfeld, K.: Global Carbon and other Biogeochemical Cycles and Feedbacks, Cambridge University Press, Cambridge, United Kingdom and New York, NY, USA, https://doi.org/10.1017/9781009157896.007, 2021.

Cheruy, F., Ducharne, A., Hourdin, F., Musat, I., Vignon, É., Gastineau, G., Bastrikov, V., Vuichard, N., Diallo, B., Dufresne, J.-L., et al.: Improved near-surface continental climate in IPSL-CM6A-LR by combined evolutions of atmospheric and land surface physics, Journal of Advances in Modeling Earth Systems, 12, e2019MS002 005, 2020.

Clark, D., Mercado, L., Sitch, S., Jones, C., Gedney, N., Best, M., Pryor, M., Rooney, G., Essery, R., Blyth, E., et al.: The Joint UK Land Environment Simulator (JULES), model description–Part 2: carbon fluxes and vegetation dynamics, Geoscientific Model Development, 4, 701–722, 2011.

Cox, P. M., Betts, R. A., Jones, C. D., Spall, S. A., and Totterdell, I. J.: Acceleration of global warming due to carbon-cycle feedbacks in a coupled climate model, Nature, 408, 184, 2000.

Crowther, T. W., Todd-Brown, K. E., Rowe, C. W., Wieder, W. R., Carey, J. C., Machmuller, M. B., Snoek, B., Fang, S., Zhou, G., Allison, S. D., et al.: Quantifying global soil carbon losses in response to warming, Nature, 540, 104, 2016.

Dai, Y., Zeng, X., Dickinson, R. E., Baker, I., Bonan, G. B., Bosilovich, M. G., Denning, A. S., Dirmeyer, P. A., Houser, P. R., Niu, G., et al.: The common land model, Bulletin of the American Meteorological Society, 84, 1013–1024, 2003.

Danabasoglu, G., Lamarque, J.-F., Bacmeister, J., Bailey, D., DuVivier, A., Edwards, J., Emmons, L., Fasullo, J., Garcia, R., Gettelman, A., et al.: The community earth system model version 2 (CESM2), Journal of Advances in Modeling Earth Systems, 12, 2020.

Davies-Barnard, T., Meyerholt, J., Zaehle, S., Friedlingstein, P., Brovkin, V., Fan, Y., Fisher, R. A., Jones, C. D., Lee, H., Peano, D., et al.: Nitrogen cycling in CMIP6 land surface models: progress and limitations, Biogeosciences, 17, 5129–5148, 2020.

Delire, C., Séférian, R., Decharme, B., Alkama, R., Calvet, J.-C., Carrer, D., Gibelin, A.-L., Joetzjer, E., Morel, X., Rocher, M., et al.: The global land carbon cycle simulated with ISBA-CTRIP: Improvements over the last decade, Journal of Advances in Modeling Earth Systems, 12, e2019MS001 886, 2020.

Dufresne, J.-L., Foujols, M.-A., Denvil, S., Caubel, A., Marti, O., Aumont, O., Balkanski, Y., Bekki, S., Bellenger, H., Benshila, R., et al.: Climate change projections using the IPSL-CM5 Earth System Model: from CMIP3 to CMIP5, Climate dynamics, 40, 2123–2165, 2013.

Dunne, J., Horowitz, L., Adcroft, A., Ginoux, P., Held, I., John, J., Krasting, J., Malyshev, S., Naik, V., Paulot, F., et al.: The GFDL Earth System Model version 4.1 (GFDL-ESM 4.1): Overall coupled model description and simulation characteristics, Journal of Advances in Modeling Earth Systems, 12, e2019MS002 015, 2020.

Dunne, J. P., John, J. G., Adcroft, A. J., Griffies, S. M., Hallberg, R. W., Shevliakova, E., Stouffer, R. J., Cooke, W., Dunne, K. A., Harrison, M. J., et al.: GFDL's ESM2 global coupled climate–carbon earth system models. Part I: Physical formulation and baseline simulation characteristics, Journal of climate, 25, 6646–6665, 2012.

Dunne, J. P., John, J. G., Shevliakova, E., Stouffer, R. J., Krasting, J. P., Malyshev, S. L., Milly, P., Sentman, L. T., Adcroft, A. J., Cooke, W., et al.: GFDL's ESM2 global coupled climate–carbon earth system models. Part II: carbon system formulation and baseline simulation characteristics, Journal of Climate, 26, 2247–2267, 2013.

Exbrayat, J.-F., Pitman, A., Zhang, Q., Abramowitz, G., and Wang, Y.-P.: Examining soil carbon uncertainty in a global model: response of microbial decomposition to temperature, moisture and nutrient limitation, Biogeosciences, 10, 7095–7108, 2013.

Eyring, V., Bony, S., Meehl, G. A., Senior, C. A., Stevens, B., Stouffer, R. J., and Taylor, K. E.: Overview of the Coupled Model Intercomparison Project Phase 6 (CMIP6) experimental design and organization, Geoscientific Model Development (Online), 9, 2016.

Friedlingstein, P., Cox, P., Betts, R., Bopp, L., von Bloh, W., Brovkin, V., Cadule, P., Doney, S., Eby, M., Fung, I., et al.: Climate–carbon cycle feedback analysis: results from the C4MIP model intercomparison, Journal of climate, 19, 3337–3353, 2006.

Friedlingstein, P., O'sullivan, M., Jones, M. W., Andrew, R. M., Gregor, L., Hauck, J., Le Quéré, C., Luijkx, I. T., Olsen, A., Peters, G. P., et al.: Global carbon budget 2022, Earth System Science Data, 14, 4811–4900, 2022.

Goll, D. S., Brovkin, V., Liski, J., Raddatz, T., Thum, T., and Todd-Brown, K. E.: Strong dependence of CO2 emissions from anthropogenic land cover change on initial land cover and soil carbon parametrization, Global Biogeochemical Cycles, 29, 1511–1523, 2015.

Goll, D. S., Winkler, A. J., Raddatz, T., Dong, N., Prentice, I. C., Ciais, P., and Brovkin, V.: Carbon–nitrogen interactions in idealized simulations with JSBACH (version 3.10), Geoscientific Model Development, 10, 2009–2030, 2017.

Green, J. K., Seneviratne, S. I., Berg, A. M., Findell, K. L., Hagemann, S., Lawrence, D. M., and Gentine, P.: Large influence of soil moisture on long-term terrestrial carbon uptake, Nature, 565, 476–479, 2019.

Guimberteau, M., Zhu, D., Maignan, F., Huang, Y., Yue, C., Dantec-Nédélec, S., Ottlé, C., Jornet-Puig, A., Bastos, A., Laurent, P., et al.: ORCHIDEE-MICT (v8. 4.1), a land surface model for the high latitudes: model description and validation, Geoscientific Model Development, 11, 121–163, 2018.

Hajima, T., Watanabe, M., Yamamoto, A., Tatebe, H., Noguchi, M. A., Abe, M., Ohgaito, R., Ito, A., Yamazaki, D., Okajima, H., et al.: Development of the MIROC-ES2L Earth system model and the evaluation of biogeochemical processes and feedbacks, Geoscientific Model Development, 13, 2197–2244, 2020.

Haverd, V., Smith, B., Nieradzik, L., Briggs, P. R., Woodgate, W., Trudinger, C. M., Canadell, J. G., and Cuntz, M.: A new version of the CABLE land surface model (Subversion revision r4601) incorporating land use and land cover change, woody vegetation demography, and a novel optimisation-based approach to plant coordination of photosynthesis, Geoscientific Model Development, 11, 2995–3026, 2018.

He, Y., Trumbore, S. E., Torn, M. S., Harden, J. W., Vaughn, L. J., Allison, S. D., and Randerson, J. T.: Radiocarbon constraints imply reduced carbon uptake by soils during the 21st century, Science, 353, 1419–1424, 2016.

Hugelius, G., Loisel, J., Chadburn, S., Jackson, R. B., Jones, M., MacDonald, G., Marushchak, M., Olefeldt, D., Packalen, M., Siewert, M. B., et al.: Large stocks of peatland carbon and nitrogen are vulnerable to permafrost thaw, Proceedings of the National Academy of Sciences, 117, 20 438–20 446, 2020.

Ito, A. and Oikawa, T.: A simulation model of the carbon cycle in land ecosystems (Sim-CYCLE): a description based on dry-matter production theory and plot-scale validation, Ecological modelling, 151, 143–176, 2002.

Iversen, T., Bentsen, M., Bethke, I., Debernard, J., Kirkevåg, A., Seland, Ø., Drange, H., Kristjansson, J., Medhaug, I., Sand, M., et al.: The Norwegian earth system model, NorESM1-M–Part 2: climate response and scenario projections, Geoscientific Model Development, 6, 389–415, 2013.

Jackson, R. B., Lajtha, K., Crow, S. E., Hugelius, G., Kramer, M. G., and Piñeiro, G.: The ecology of soil carbon: pools, vulnerabilities, and biotic and abiotic controls, Annual Review of Ecology, Evolution, and Systematics, 48, 419–445, 2017.

Jenkinson, D., Adams, D., and Wild, A.: Model estimates of CO2 emissions from soil in response to global warming, Nature, 351, 304–306, 1991.

Ji, D., Wang, L., Feng, J., Wu, Q., Cheng, H., Zhang, Q., Yang, J., Dong, W., Dai, Y., Gong, D., et al.: Description and basic evaluation of Beijing Normal University Earth system model (BNU-ESM) version 1, Geoscientific Model Development, 7, 2039–2064, 2014.

Ji, J., Huang, M., and Li, K.: Prediction of carbon exchanges between China terrestrial ecosystem and atmosphere in 21st century, Science in China Series D: Earth Sciences, 51, 885–898, 2008.

Jones, C., Hughes, J., Bellouin, N., Hardiman, S., Jones, G., Knight, J., Liddicoat, S., O'connor, F., Andres, R. J., Bell, C., et al.: The HadGEM2-ES implementation of CMIP5 centennial simulations, Geoscientific Model Development, 4, 543–570, 2011.

Jones, C. D., Arora, V., Friedlingstein, P., Bopp, L., Brovkin, V., Dunne, J., Graven, H., Hoffman, F., Ilyina, T., John, J. G., et al.: C4MIP–The coupled climate–carbon cycle model intercomparison project: Experimental protocol for CMIP6, Geoscientific Model Development, 9, 2853–2880, 2016.

Knorr, W.: Annual and interannual CO2 exchanges of the terrestrial biosphere: Process-based simulations and uncertainties, Global Ecology and Biogeography, 9, 225–252, 2000.

Koven, C. D., Chambers, J. Q., Georgiou, K., Knox, R., Negron-Juarez, R., Riley, W. J., Arora, V. K., Brovkin, V., Friedlingstein, P., and Jones, C. D.: Controls on terrestrial carbon feedbacks by productivity versus turnover in the CMIP5 Earth System Models, Biogeosciences, 12, 5211–5228, https://doi.org/10.5194/bg-12-5211-2015, 2015.

Krinner, G., Viovy, N., de Noblet-Ducoudré, N., Ogée, J., Polcher, J., Friedlingstein, P., Ciais, P., Sitch, S., and Prentice, I. C.: A dynamic global vegetation model for studies of the coupled atmosphere-biosphere system, Global Biogeochemical Cycles, 19, 2005.

Lawrence, D. M., Oleson, K. W., Flanner, M. G., Thornton, P. E., Swenson, S. C., Lawrence, P. J., Zeng, X., Yang, Z.-L., Levis, S., Sakaguchi, K., et al.: Parameterization improvements and functional and structural advances in version 4 of the Community Land Model, Journal of Advances in Modeling Earth Systems, 3, 2011.

Lawrence, D. M., Fisher, R. A., Koven, C. D., Oleson, K. W., Swenson, S. C., Bonan, G., Collier, N., Ghimire, B., Van Kampenhout, L., Kennedy, D., et al.: The Community Land Model version 5: Description of new features, benchmarking, and impact of forcing uncertainty, Journal of Advances in Modeling Earth Systems, 11, 4245–4287, 2019.

Liu, X.-J. A., Finley, B. K., Mau, R. L., Schwartz, E., Dijkstra, P., Bowker, M. A., and Hungate, B. A.: The soil priming effect: Consistent across ecosystems, elusive mechanisms, Soil Biology and Biochemistry, 140, 107 617, 2020.

Mauritsen, T., Bader, J., Becker, T., Behrens, J., Bittner, M., Brokopf, R., Brovkin, V., Claussen, M., Crueger, T., Esch, M., et al.: Developments in the MPI-M Earth System Model version 1.2 (MPI-ESM1. 2) and its response to increasing CO2, Journal of Advances in Modeling Earth Systems, 11, 998–1038, 2019.

Meinshausen, M., Smith, S. J., Calvin, K., Daniel, J. S., Kainuma, M., Lamarque, J.-F., Matsumoto, K., Montzka, S., Raper, S., Riahi, K., et al.: The RCP greenhouse gas concentrations and their extensions from 1765 to 2300, Climatic change, 109, 213, 2011.

Melton, J. R., Arora, V. K., Wisernig-Cojoc, E., Seiler, C., Fortier, M., Chan, E., and Teckentrup, L.: CLASSIC v1. 0: the open-source community successor to the Canadian Land Surface Scheme (CLASS) and the Canadian Terrestrial Ecosystem Model (CTEM)–Part 1: Model framework and site-level performance, Geoscientific Model Development, 13, 2825–2850, 2020.

O'Neill, B. C., Tebaldi, C., Vuuren, D. P. v., Eyring, V., Friedlingstein, P., Hurtt, G., Knutti, R., Kriegler, E., Lamarque, J.-F., Lowe, J., et al.: The scenario model intercomparison project (ScenarioMIP) for CMIP6, Geoscientific Model Development, 9, 3461–3482, 2016.

O'Neill, B. C., Kriegler, E., Riahi, K., Ebi, K. L., Hallegatte, S., Carter, T. R., Mathur, R., and van Vuuren, D. P.: A new scenario framework for climate change research: the concept of shared socioeconomic pathways, Climatic change, 122, 387–400, 2014.

Parton, W. J., Stewart, J. W., and Cole, C. V.: Dynamics of C, N, P and S in grassland soils: a model, Biogeochemistry, 5, 109–131, 1988.

Raddatz, T., Reick, C., Knorr, W., Kattge, J., Roeckner, E., Schnur, R., Schnitzler, K.-G., Wetzel, P., and Jungclaus, J.: Will the tropical land biosphere dominate the climate–carbon cycle feedback during the twenty-first century?, Climate dynamics, 29, 565–574, 2007.

Sato, H., Itoh, A., and Kohyama, T.: SEIB–DGVM: A new Dynamic Global Vegetation Model using a spatially explicit individual-based approach, Ecological Modelling, 200, 279–307, 2007.

Schimel, D., Stephens, B. B., and Fisher, J. B.: Effect of increasing CO2 on the terrestrial carbon cycle, Proceedings of the National Academy of Sciences, 112, 436–441, 2015.

Schmidt, G. A., Kelley, M., Nazarenko, L., Ruedy, R., Russell, G. L., Aleinov, I., Bauer, M., Bauer, S. E., Bhat, M. K., Bleck, R., et al.: Configuration and assessment of the GISS ModelE2 contributions to the CMIP5 archive, Journal of Advances in Modeling Earth Systems, 6, 141–184, 2014.

Schmidt, M. W., Torn, M. S., Abiven, S., Dittmar, T., Guggenberger, G., Janssens, I. A., Kleber, M., Kögel-Knabner, I., Lehmann, J., Manning, D. A., et al.: Persistence of soil organic matter as an ecosystem property, Nature, 478, 49–56, 2011.

Schuur, E. A., Abbott, B. W., Commane, R., Ernakovich, J., Euskirchen, E., Hugelius, G., Grosse, G., Jones, M., Koven, C., Leshyk, V., et al.: Permafrost and climate change: carbon cycle feedbacks from the warming Arctic, Annual Review of Environment and Resources, 47, 343–371, 2022.

Séférian, R., Nabat, P., Michou, M., Saint-Martin, D., Voldoire, A., Colin, J., Decharme, B., Delire, C., Berthet, S., Chevallier, M., et al.: Evaluation of CNRM earth system model, CNRM-ESM2-1: Role of earth system processes in present-day and future climate, Journal of Advances in Modeling Earth Systems, 11, 4182–4227, 2019.

Seiler, C., Melton, J. R., Arora, V. K., and Wang, L.: CLASSIC v1. 0: the open-source community successor to the Canadian Land Surface Scheme (CLASS) and the Canadian Terrestrial Ecosystem Model (CTEM)–Part 2: Global benchmarking, Geoscientific Model Development, 14, 2371–2417, 2021.

Seland, Ø., Bentsen, M., Olivié, D., Toniazzo, T., Gjermundsen, A., Graff, L. S., Debernard, J. B., Gupta, A. K., He, Y.-C., Kirkevåg, A., et al.: Overview of the Norwegian Earth System Model (NorESM2) and key climate response of CMIP6 DECK, historical, and scenario simulations, Geoscientific Model Development, 13, 6165–6200, 2020.

Sellar, A. A., Walton, J., Jones, C. G., Wood, R., Abraham, N. L., Andrejczuk, M., Andrews, M. B., Andrews, T., Archibald, A. T., de Mora, L., et al.: Implementation of UK Earth system models for CMIP6, Journal of Advances in Modeling Earth Systems, 12, e2019MS001 946, 2020.

Shevliakova, E., Pacala, S. W., Malyshev, S., Hurtt, G. C., Milly, P., Caspersen, J. P., Sentman, L. T., Fisk, J. P., Wirth, C., and Crevoisier, C.: Carbon cycling under 300 years of land use change: Importance of the secondary vegetation sink, Global Biogeochemical Cycles, 23, 2009.

Shi, Z., Allison, S. D., He, Y., Levine, P. A., Hoyt, A. M., Beem-Miller, J., Zhu, Q., Wieder, W. R., Trumbore, S., and Randerson, J. T.: The age distribution of global soil carbon inferred from radiocarbon measurements, Nature Geoscience, 13, 555–559, 2020.

Sierra, C. A., Trumbore, S. E., Davidson, E. A., Vicca, S., and Janssens, I.: Sensitivity of decomposition rates of soil organic matter with respect to simultaneous changes in temperature and moisture, Journal of Advances in Modeling Earth Systems, 7, 335–356, 2015.

Swart, N. C., Cole, J. N., Kharin, V. V., Lazare, M., Scinocca, J. F., Gillett, N. P., Anstey, J., Arora, V., Christian, J. R., Hanna, S., et al.: The Canadian earth system model version 5 (CanESM5. 0.3), Geoscientific Model Development, 12, 4823–4873, 2019.

Taylor, K. E., Stouffer, R. J., and Meehl, G. A.: An overview of CMIP5 and the experiment design, Bulletin of the American Meteorological Society, 93, 485–498, 2012.

Todd-Brown, K., Randerson, J., Post, W., Hoffman, F., Tarnocai, C., Schuur, E., and Allison, S.: Causes of variation in soil carbon simulations from CMIP5 Earth system models and comparison with observations, Biogeosciences, 10, 1717–1736, 2013.

Todd-Brown, K., Randerson, J., Hopkins, F., Arora, V., Hajima, T., Jones, C., Shevliakova, E., Tjiputra, J., Volodin, E., Wu, T., et al.: Changes in soil organic carbon storage predicted by Earth system models during the 21st century, Biogeosciences, 11, 2341–2356, 2014.

Todd-Brown, K., Zheng, B., and Crowther, T. W.: Field-warmed soil carbon changes imply high 21st-century<? xmltex\break?> modeling uncertainty, Biogeosciences, 15, 3659–3671, 2018.

Van Gestel, N., Shi, Z., Van Groenigen, K. J., Osenberg, C. W., Andresen, L. C., Dukes, J. S., Hovenden, M. J., Luo, Y., Michelsen, A., Pendall, E., et al.: Predicting soil carbon loss with warming, Nature, 554, E4–E5, 2018.

Varney, R. M., Chadburn, S. E., Friedlingstein, P., Burke, E. J., Koven, C. D., Hugelius, G., and Cox, P. M.: A spatial emergent constraint on the sensitivity of soil carbon turnover to global warming, Nature communications, 11, 1–8, 2020.

Varney, R. M., Chadburn, S. E., Burke, E. J., and Cox, P. M.: Evaluation of soil carbon simulation in CMIP6 Earth system models, Biogeosciences, 19, 4671–4704, https://doi.org/10.5194/bg-19-4671-2022, 2022.

Watanabe, S., Hajima, T., Sudo, K., Nagashima, T., Takemura, T., Okajima, H., Nozawa, T., Kawase, H., Abe, M., Yokohata, T., et al.: MIROC-ESM 2010: Model description and basic results of CMIP5-20c3m experiments, Geoscientific Model Development, 4, 845–872, 2011.

Wieder, W. R., Allison, S. D., Davidson, E. A., Georgiou, K., Hararuk, O., He, Y., Hopkins, F., Luo, Y., Smith, M. J., Sulman, B., et al.: Explicitly representing soil microbial processes in Earth system models, Global Biogeochemical Cycles, 29, 1782–1800, 2015a.

Wieder, W. R., Cleveland, C. C., Smith, W. K., and Todd-Brown, K.: Future productivity and carbon storage limited by terrestrial nutrient availability, Nature Geoscience, 8, 441–444, 2015b.

Wiltshire, A. J., Burke, E. J., Chadburn, S. E., Jones, C. D., Cox, P. M., Davies-Barnard, T., Friedlingstein, P., Harper, A. B., Liddicoat, S., Sitch, S., et al.: JULES-CN: a coupled terrestrial carbon–nitrogen scheme (JULES vn5. 1), Geoscientific Model Development, 14, 2161–2186, 2021.

Wu, T., Lu, Y., Fang, Y., Xin, X., Li, L., Li, W., Jie, W., Zhang, J., Liu, Y., Zhang, L., et al.: The Beijing Climate Center climate system model (BCC-CSM): The main progress from CMIP5 to CMIP6, Geoscientific Model Development, 12, 1573–1600, 2019.

Yue, X. and Unger, N.: The Yale Interactive terrestrial Biosphere model version 1.0: description, evaluation and implementation into NASA GISS ModelE2, Geoscientific Model Development, 8, 2399–2417, 2015.

Zhao, M., Golaz, J.-C., Held, I., Guo, H., Balaji, V., Benson, R., Chen, J.-H., Chen, X., Donner, L., Dunne, J., et al.: The GFDL global atmosphere and land model AM4. 0/LM4. 0: 2. Model description, sensitivity studies, and tuning strategies, Journal of Advances in Modeling Earth Systems, 10, 735–769, 2018.

Ziehn, T., Chamberlain, M. A., Law, R. M., Lenton, A., Bodman, R. W., Dix, M., Stevens, L., Wang, Y.-P., and Srbinovsky, J.: The Australian Earth System Model: ACCESS-ESM1. 5, Journal of Southern Hemisphere Earth Systems Science, 70, 193–214, 2020.

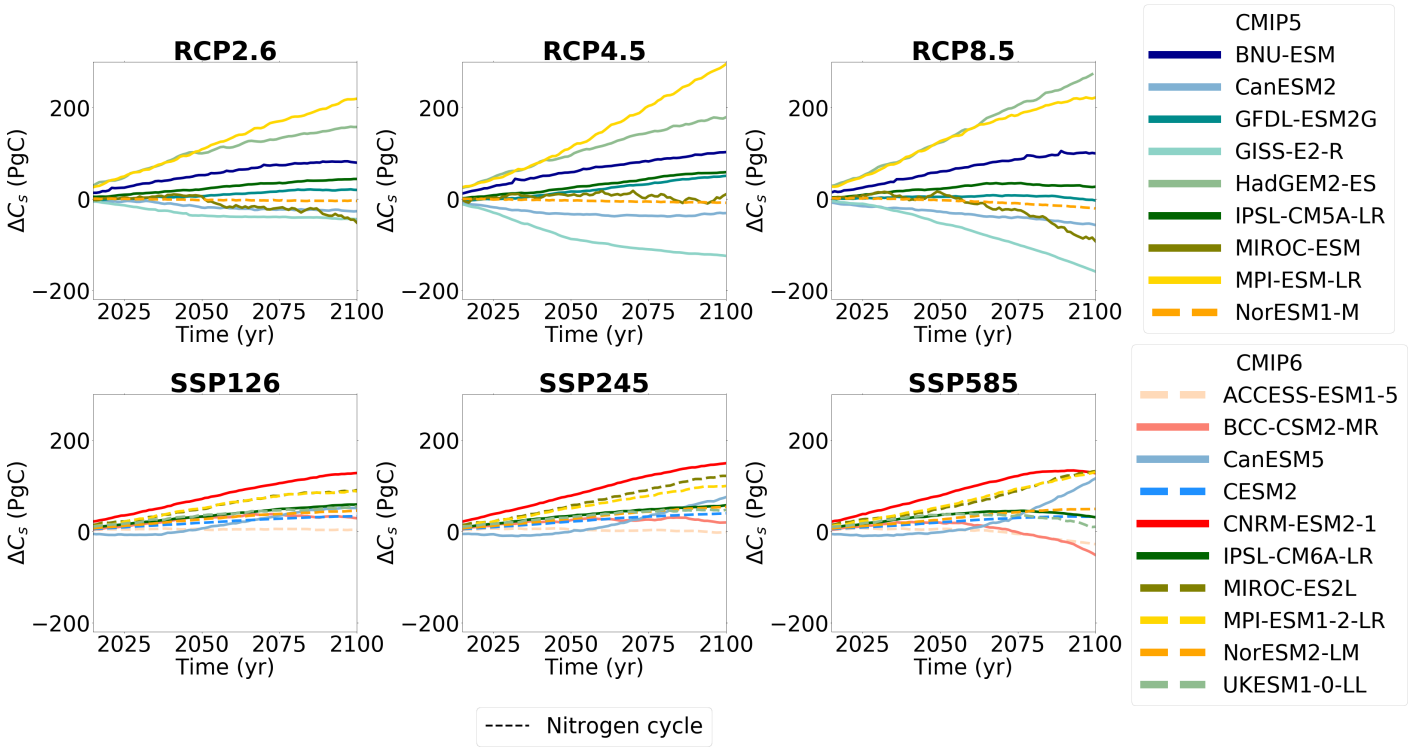

Figure 1. Projected future change in soil carbon (ΔC_s) in CMIP5 (top row) and CMIP6 (bottom row) ESMs, for future climate scenarios *RCP2.6* and *SSP126*, *RCP4.5* and *SSP245*, *RCP8.5* and *SSP585*, respectively. The dashed lines represent ESMs which include the representation of interactive nitrogen in these simulations.

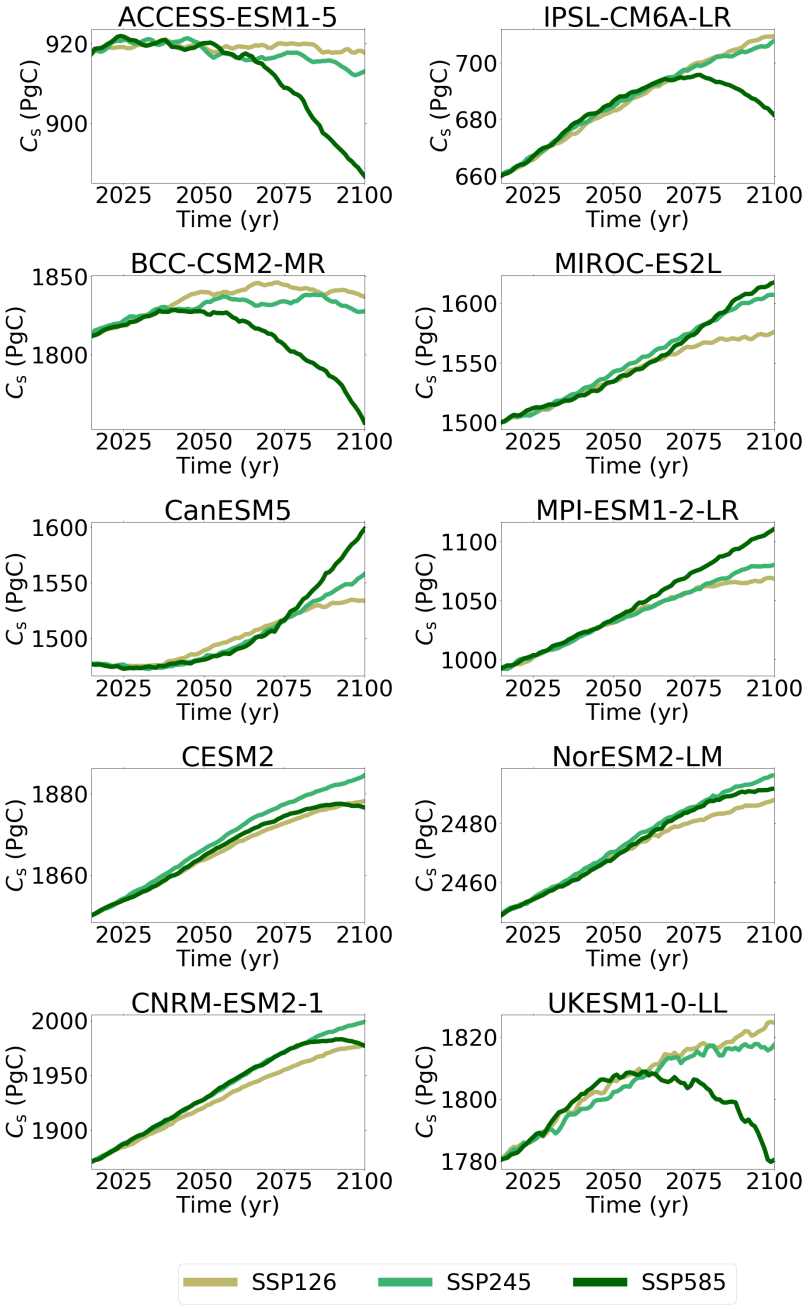

Figure 2. Timeseries of projected future soil carbon (C_s) in CMIP6 ESMs for future climate scenarios *SSP126*, *SSP245*, *SSP585*.

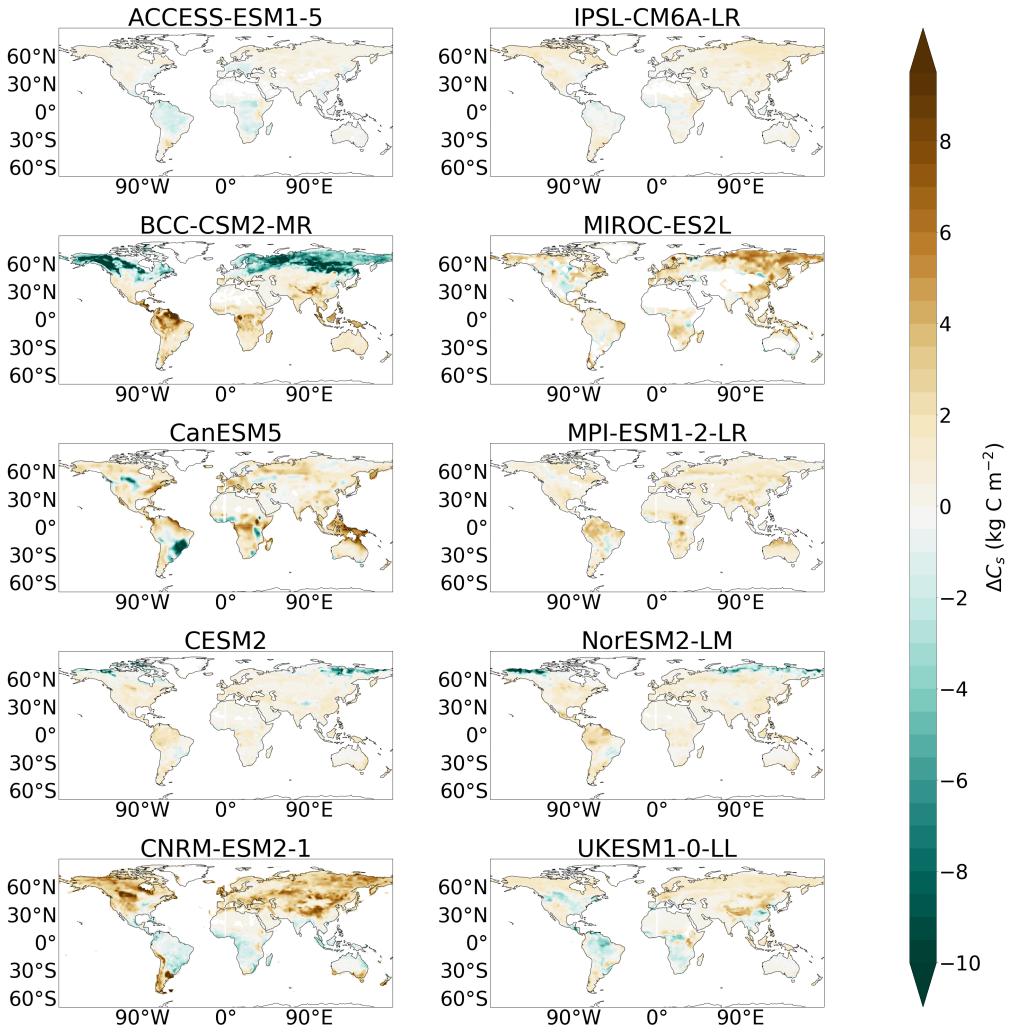

Figure 3. Map plots showing the change in soil carbon (ΔC_s) in *SSP585* for each CMIP6 ESM.

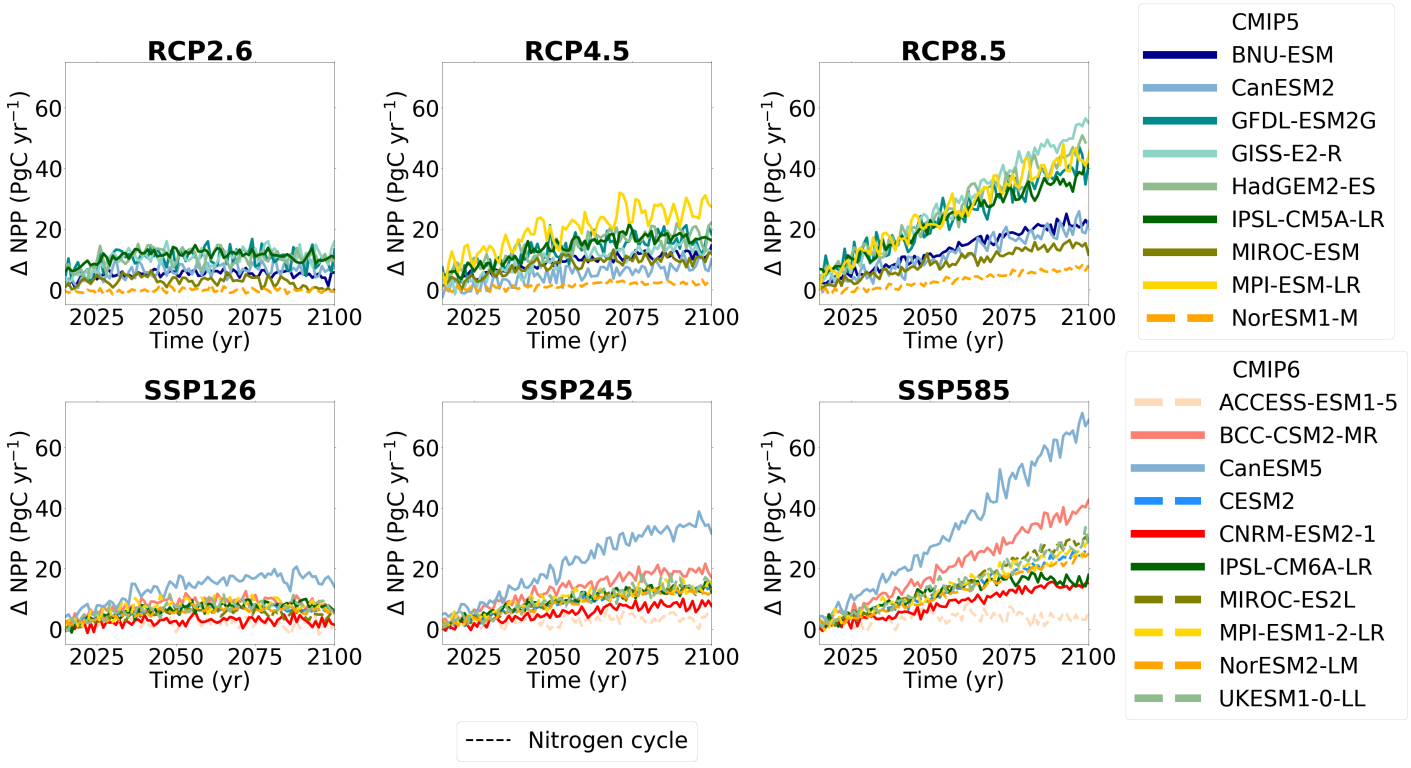

Figure 4. Projected future change in Net Primary Production (ΔNPP) in CMIP5 (top row) and CMIP6 (bottom row) ESMs, for future climate scenarios *RCP2.6* and *SSP126*, *RCP4.5* and *SSP245*, *RCP8.5* and *SSP585*, respectively. The dashed lines represent ESMs which include the representation of interactive nitrogen in these simulations.

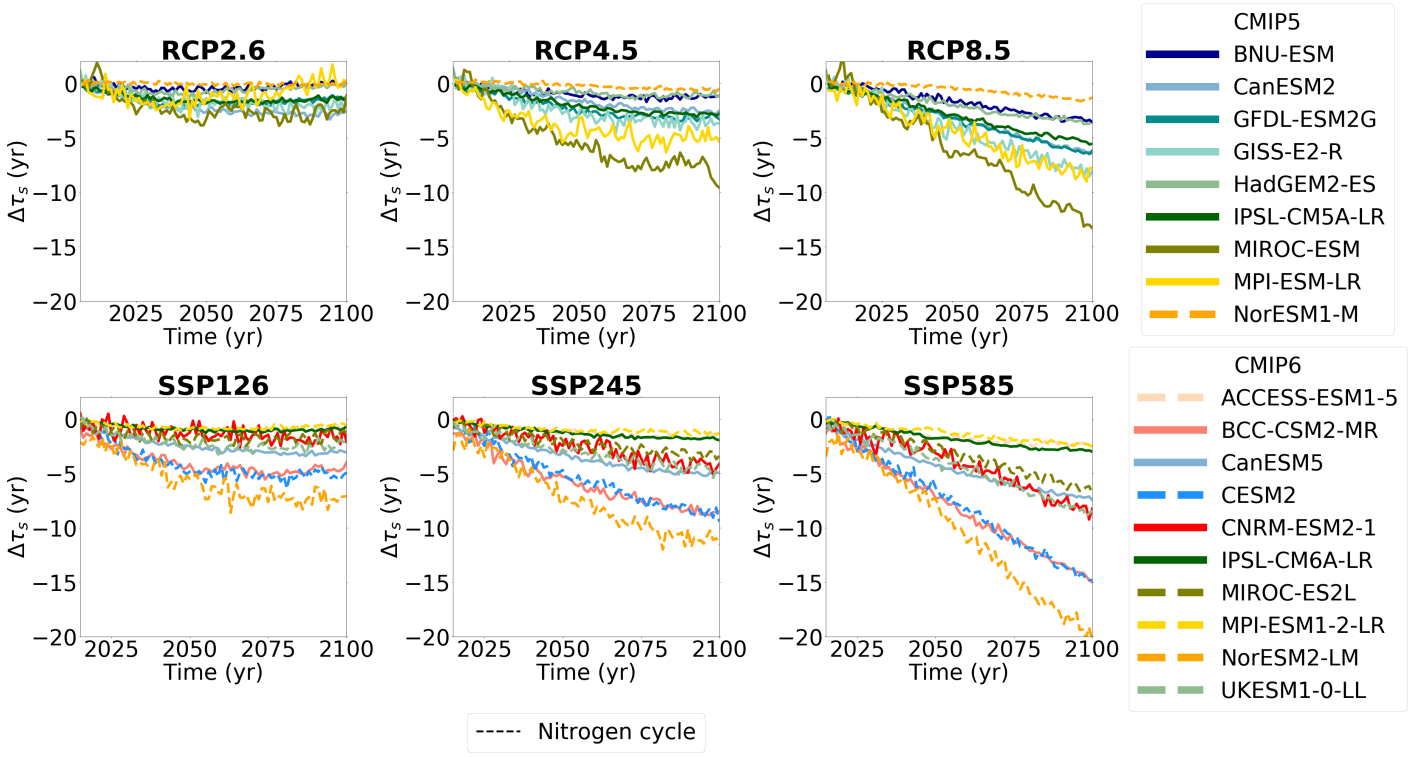

Figure 5. Projected future change in soil carbon turnover time ($\Delta\tau_s$) in CMIP5 (top row) and CMIP6 (bottom row) ESMs, for future climate scenarios *RCP2.6* and *SSP126*, *RCP4.5* and *SSP245*, *RCP8.5* and *SSP585*, respectively. The dashed lines represent ESMs which include the representation of interactive nitrogen in these simulations.

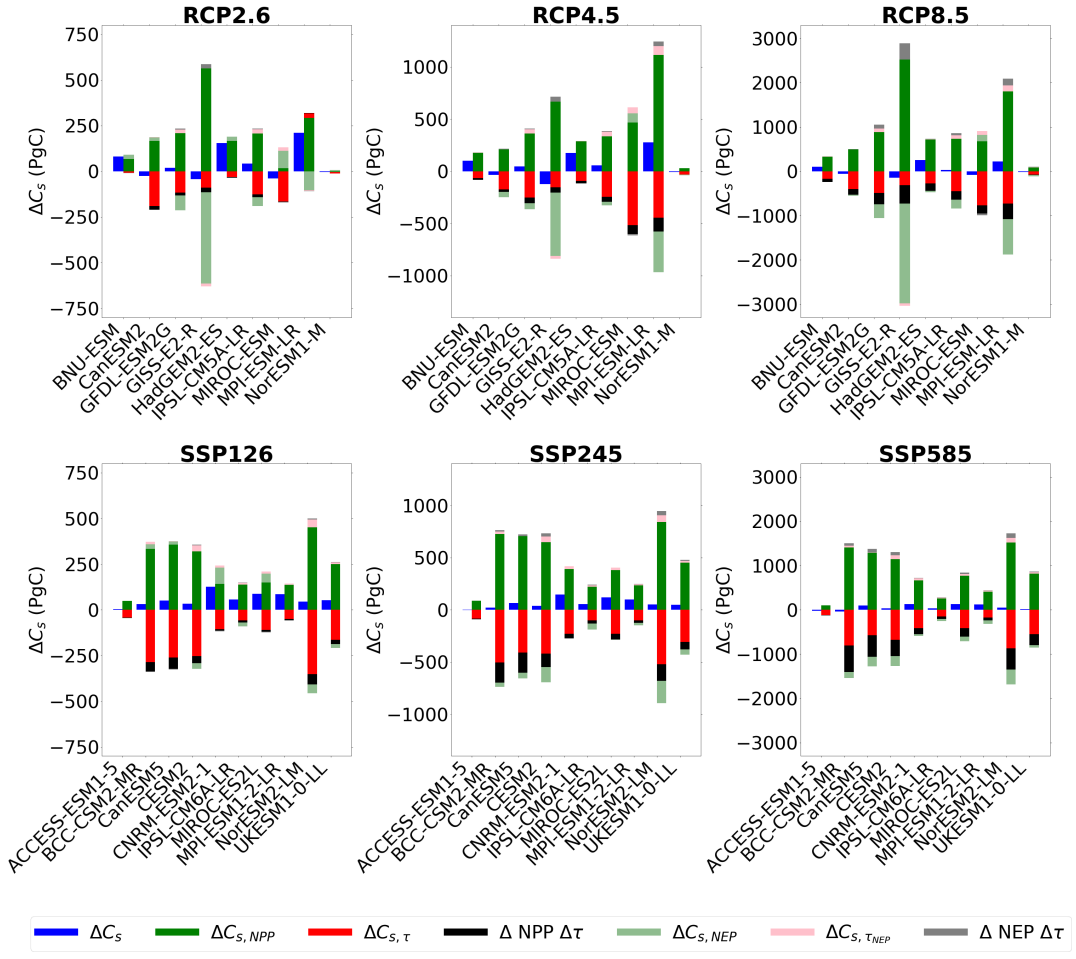

Figure 6. A bar chart showing the contributions of NPP and τ_s to end of 21$^{\text{st}}$ century changes in soil carbon (ΔC_s) in CMIP5 (top row) and CMIP6 (bottom row) ESMs, for future scenarios: *RCP2.6* and *SSP126*, *RCP4.5* and *SSP245*, *RCP8.5* and *SSP585*, respectively. The included terms are: the linear term representing changes in soil carbon due to the changes in NPP ($\Delta C_{s,NPP}$), the linear term representing changes in soil carbon due to the changes in τ_s ($\Delta C_{s,\tau}$), the non-linear term ($\Delta\text{NPP}\Delta\tau_\text{s}$), and then additional terms to account for the non-equilibrium climate in 2100 ($\Delta C_{s,NEP}$, $\Delta C_{s,\tau_{NEP}}$, and $\Delta\text{NEP}\Delta\tau_\text{s}$).

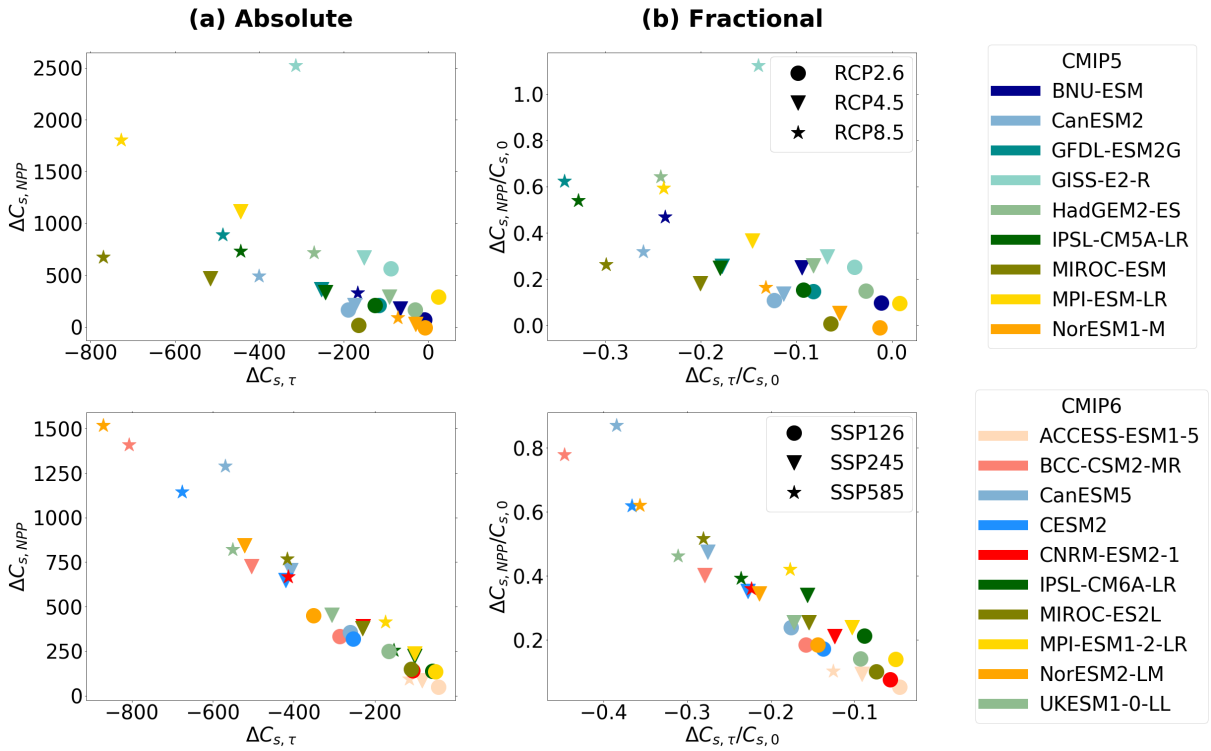

Figure 7. Scatter plot comparing the relationship between $\Delta C_{s,NPP}$ and $\Delta C_{s,\tau}$ for CMIP5 (top row) and CMIP6 (bottom row) ESMs in future scenarios *RCP2.6* and *SSP126*, *RCP4.5* and *SSP245*, *RCP8.5* and *SSP585*, respectively, for (a) absolute changes, and (b) fractional changes.

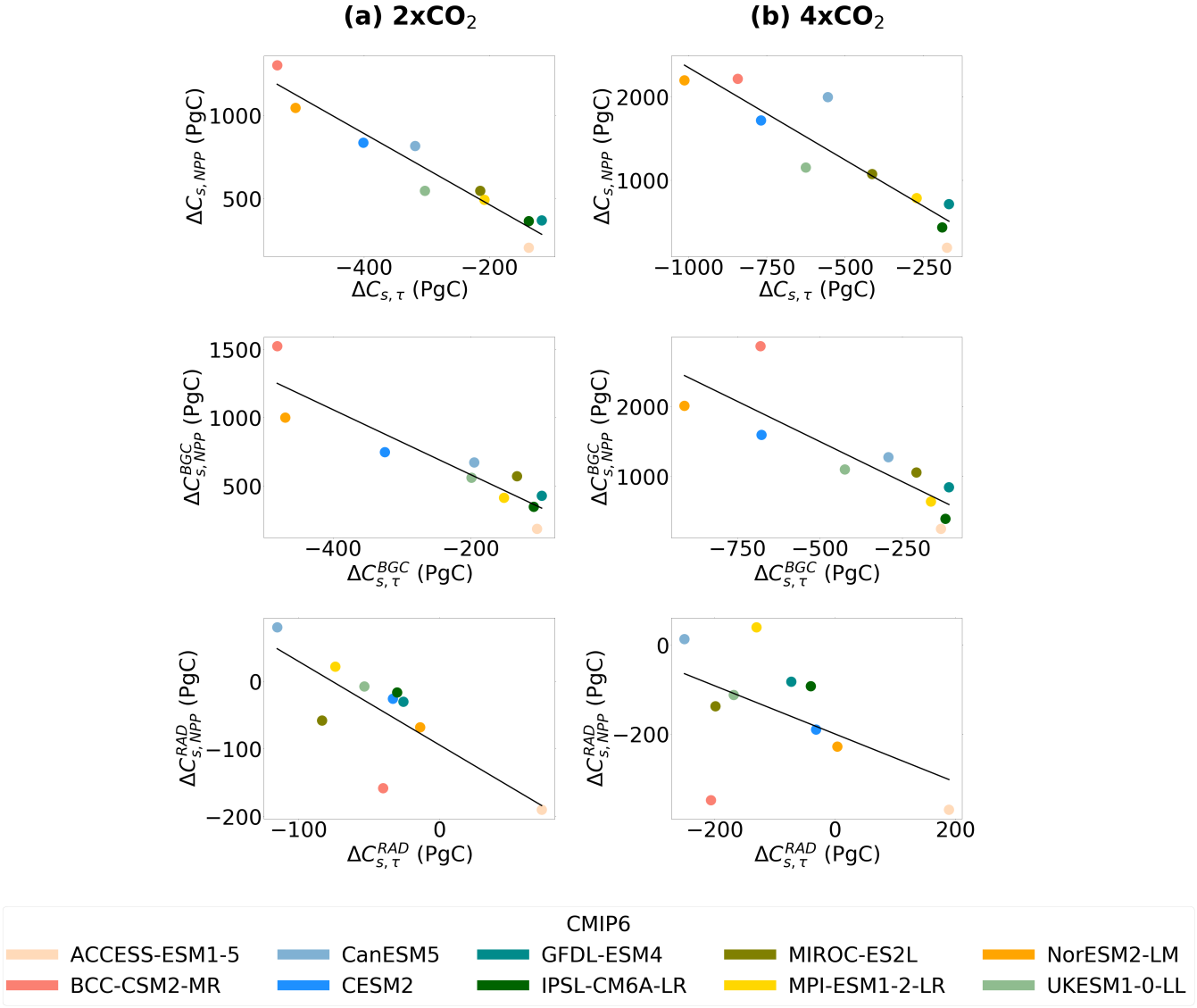

Figure 8. Scatter plots showing the relationship between $\Delta C_{s,NPP}$ and $\Delta C_{s,\tau}$ for each CMIP6 ESM, in the *full* 1% CO_2 simulation (top row), *BGC* simulation (middle row) and *RAD* simulation (bottom row), for (a) 2xCO_2 and (b) 4xCO_2.

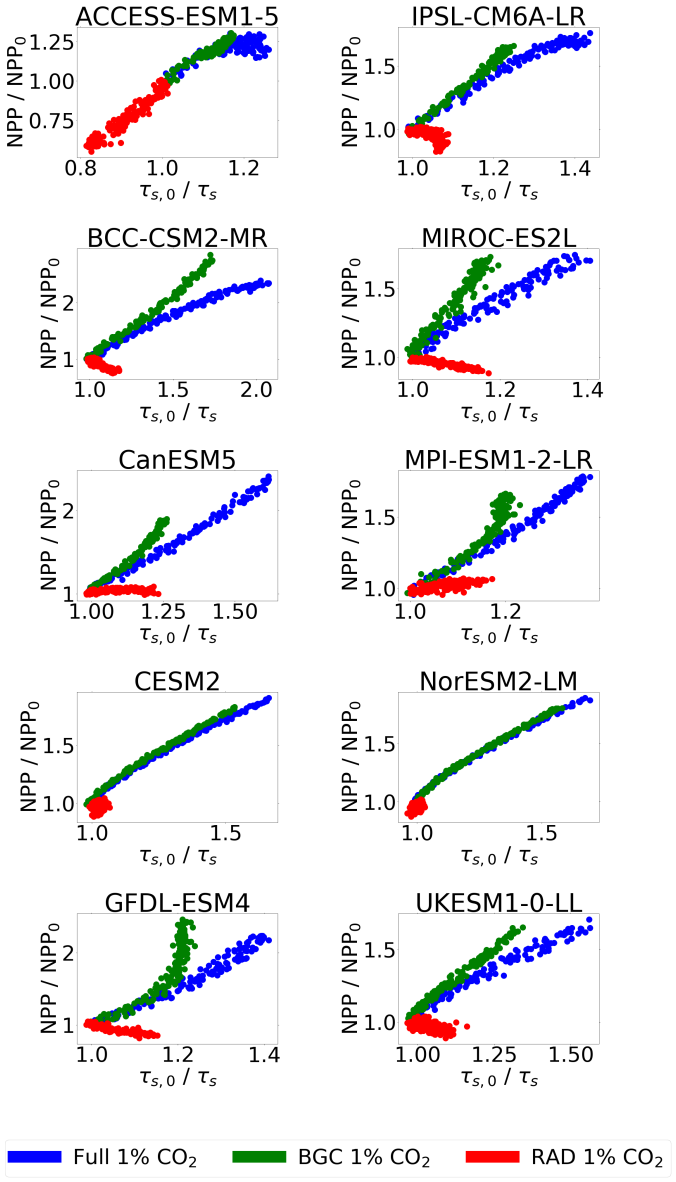

Figure 9. Scatter plots showing the correlation between $\mathrm{NPP}/\mathrm{NPP}_0$ and $\tau_{s,0}/\tau_s$ for each CMIP6 ESM, in the *full* 1% CO_2 simulation (blue) and the *BGC* simulation (green), up to 4xCO_2.

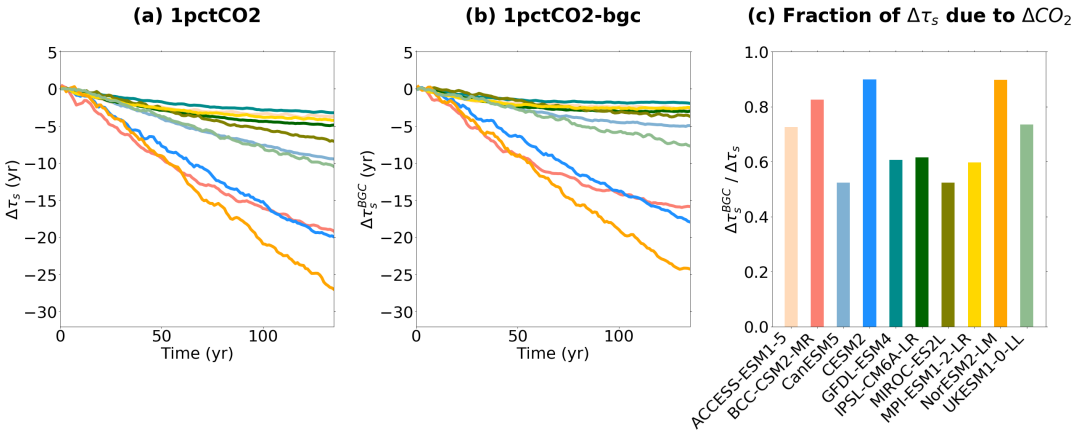

Figure 10. Changes in soil carbon turnover ($\Delta\tau_s$) in C4MIP runs for the CMIP6 ESMs, with and without direct climate effects on τ_s. (a) timeseries of $\Delta\tau_s$ in *full* 1% CO_2 simulation (climate and CO_2 changes), (b) timeseries of $\Delta\tau_s$ in *BGC* simulation (CO_2 changes only), and (c) bar chart showing the fraction of total $\Delta\tau_s$ due to the changes in CO_2 at 4xCO_2 for each model.

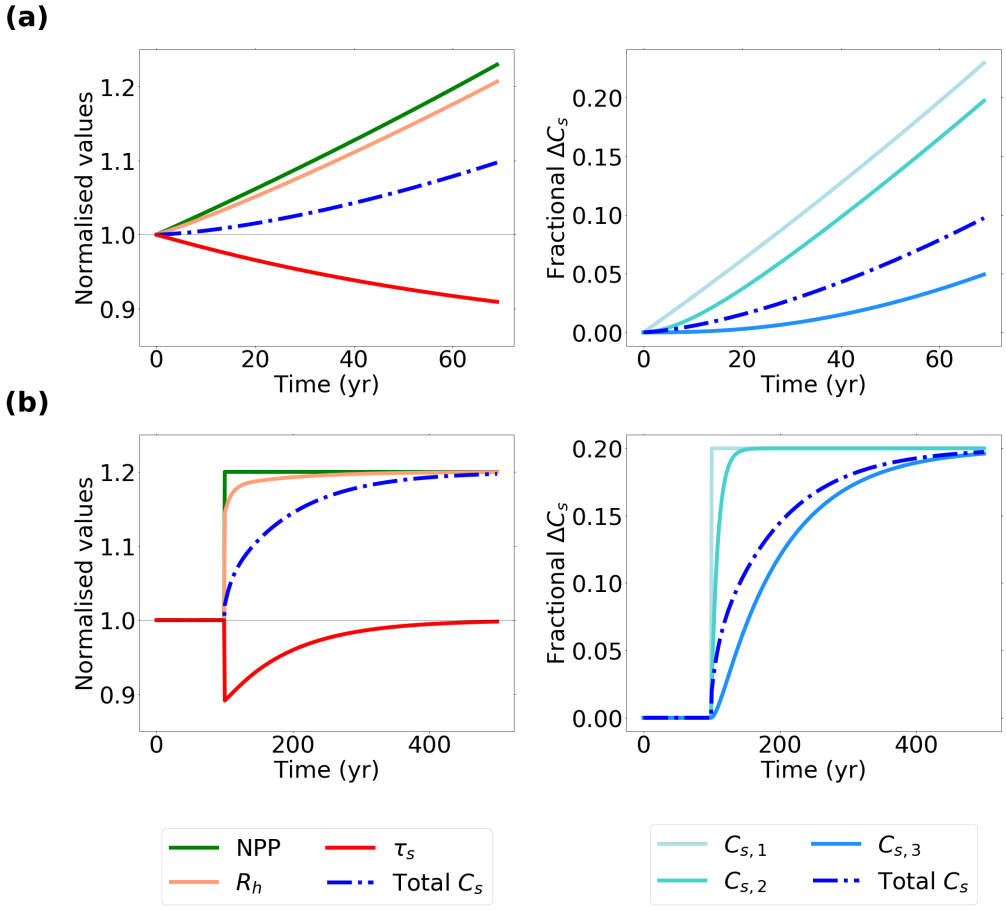

Figure 11. Timeseries plot showing the results from the simple three-box model. (a) For normalised changes in NPP, R_h, τ_s and C_s and fractional change in each of the 3 soil carbon boxes and in the total soil carbon (recreation of Fig. 12 in Koven et al. (2015)). (b) For an abrupt change in global NPP, from 50 PgC yr^{-1} to 70 PgC yr^{-1} at year 100.

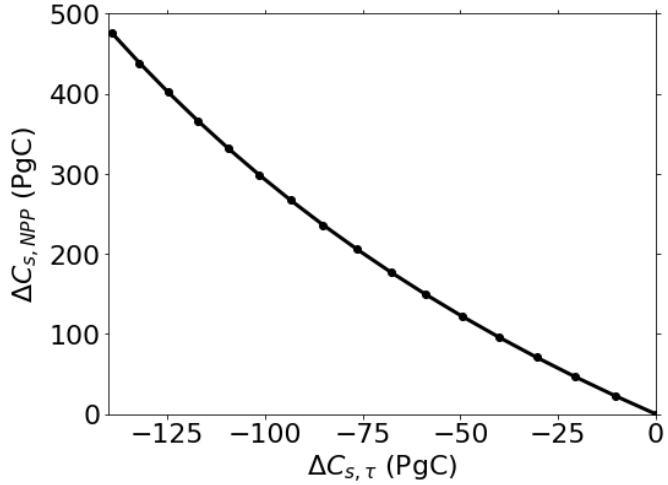

Figure 12. Relationship between $\Delta C_{s,NPP}$ and $\Delta C_{s,\tau}$ derived from the three-box model. Each dot represents the results at the end of a 70 year run with a different assumed rate of increase of NPP ($\sim$ 0.0% to 0.8% per year in increments of 0.05%).

Table 1. The CMIP5 and CMIP6 Earth system models included in this study and the relevant features of associated land carbon cycle components: simulation of interactive nitrogen, number of live carbon pools and the number of dead soil carbon pools (Varney et al., 2022; Arora et al., 2013, 2020).

Earth System Model	Nitrogen cycle	No. of live carbon pools	No. of dead carbon pools	References
BNU-ESM	No	-	-	Ji et al. (2014); Dai et al. (2003)
CanESM2	No	3	2	Arora et al. (2009); Arora and Boer (2010)
GFDL-ESM2G	No	8	2	Dunne et al. (2012, 2013); Shevliakova et al. (2009)
GISS-E2-R	No	7	5	Schmidt et al. (2014); Yue and Unger (2015)
HadGEM2-ES	No	3	4	Jones et al. (2011); Best et al. (2011); Clark et al. (2011)
IPSL-CM5A-LR	No	-	7	Dufresne et al. (2013); Krinner et al. (2005)
MIROC-ESM	No	4	2	Watanabe et al. (2011); Ito and Oikawa (2002); Sato et al. (2007)
MPI-ESM-LR	No	4	2	Raddatz et al. (2007); Knorr (2000)
NorESM1-M	Yes	13	7	Bentsen et al. (2013); Iversen et al. (2013); Lawrence et al. (2011)
ACCESS-ESM1.5	Yes	3	6	Ziehn et al. (2020); Haverd et al. (2018);
BCC-CSM2-MR	No	3	8	Wu et al. (2019); Ji et al. (2008)
CanESM5	No	3	2	Swart et al. (2019); Melton et al. (2020); Seiler et al. (2021)
CESM2	Yes	22	7	Danabasoglu et al. (2020); Lawrence et al. (2019)
CNRM-ESM2-1	No	6	7	Séférian et al. (2019); Delire et al. (2020)
GFDL-ESM4	No	6	4	Dunne et al. (2020); Zhao et al. (2018)
IPSL-CM6A-LR	No	8	3	Boucher et al. (2020); Cheruy et al. (2020); Guimberteau et al. (2018)
MIROC-ES2L	Yes	3	6	Hajima et al. (2020); Ito and Oikawa (2002)
MPI-ESM1.2-LR	Yes	3	18	Mauritsen et al. (2019); Goll et al. (2017); Goll et al. (2015)
NorESM2-LM	Yes	22	7	Seland et al. (2020); Lawrence et al. (2019)
UKESM1-0-LL	Yes	3	4	Sellar et al. (2020); Wiltshire et al. (2021)

Table 2. Table presenting the absolute (PgC) and relative (%) change in 21st century soil carbon (ΔC_s) for each CMIP6 model and the ensemble mean $\pm$ standard deviation, for each future SSP scenario.

Earth System Model	Absolute ΔC_s (PgC)			Relative ΔC_s (%)		
	SSP126	SSP245	SSP585	SSP126	SSP245	SSP585
ACCESS-ESM1.5	3.44	-0.98	-23.4	0.38	-0.108	-2.55
BCC-CSM2-MR	31.8	22.3	-35.2	1.76	1.23	-1.95
CanESM5	50.6	66.7	97.7	3.41	4.49	6.59
CESM2	32.7	38.3	32.4	1.77	2.08	1.76
CNRM-ESM2-1	126	145	132	6.79	7.85	7.11
IPSL-CM6A-LR	57.6	55.0	35.5	8.86	8.45	5.46
MIROC-ES2L	87.3	118	126	5.88	7.94	8.5
MPI-ESM1-2-LR	86.2	97.9	123	8.79	9.98	12.5
NorESM2-LM	44.1	52.0	48.7	1.81	2.13	1.99
UKESM1-0-LL	52.3	46.9	17.5	2.96	2.65	0.988
Ensemble mean	55.4	58.3	50.3	4.53	4.24	3.67
$\pm$ standard deviation	$\pm$ 31.8	$\pm$ 44.3	$\pm$ 57.8	$\pm$ 2.95	$\pm$ 3.51	$\pm$ 4.50

Table 3. Table presenting the change in 21st century NPP and τ_s for each CMIP6 model and the ensemble mean $\pm$ standard deviation, for each future SSP scenario.

Earth System Model	ΔNPP (PgC yr^{-1})			$\Delta\tau_s$ (yr)		
	SSP126	SSP245	SSP585	SSP126	SSP245	SSP585
ACCESS-ESM1.5	1.66	3.58	4.07	-0.828	-1.69	-2.35
BCC-CSM2-MR	8.37	19.7	39.4	-4.53	-8.52	-14.0
CanESM5	17.4	35.4	65.8	-3.09	-5.01	-7.10
CESM2	6.46	13.7	24.5	-5.05	-8.63	-14.1
CNRM-ESM2-1	2.28	7.96	14.3	-1.624	-4.19	-8.05
IPSL-CM6A-LR	8.40	13.9	16.2	-0.938	-1.81	-2.83
MIROC-ES2L	4.90	13.9	29.0	-1.52	-3.37	-6.23
MPI-ESM1-2-LR	7.84	14.3	25.9	-0.555	-1.27	-2.30
NorESM2-LM	6.33	12.6	23.3	-7.16	-11.0	-18.9
UKESM1-0-LL	8.08	15.2	28.1	-2.37	-4.52	-8.25
Ensemble mean	7.44	13.6	24.6	-2.30	-4.55	-7.65
$\pm$ standard deviation	$\pm$ 4.01	$\pm$ 8.71	$\pm$ 16.9	$\pm$ 2.047	$\pm$ 3.35	$\pm$ 5.65

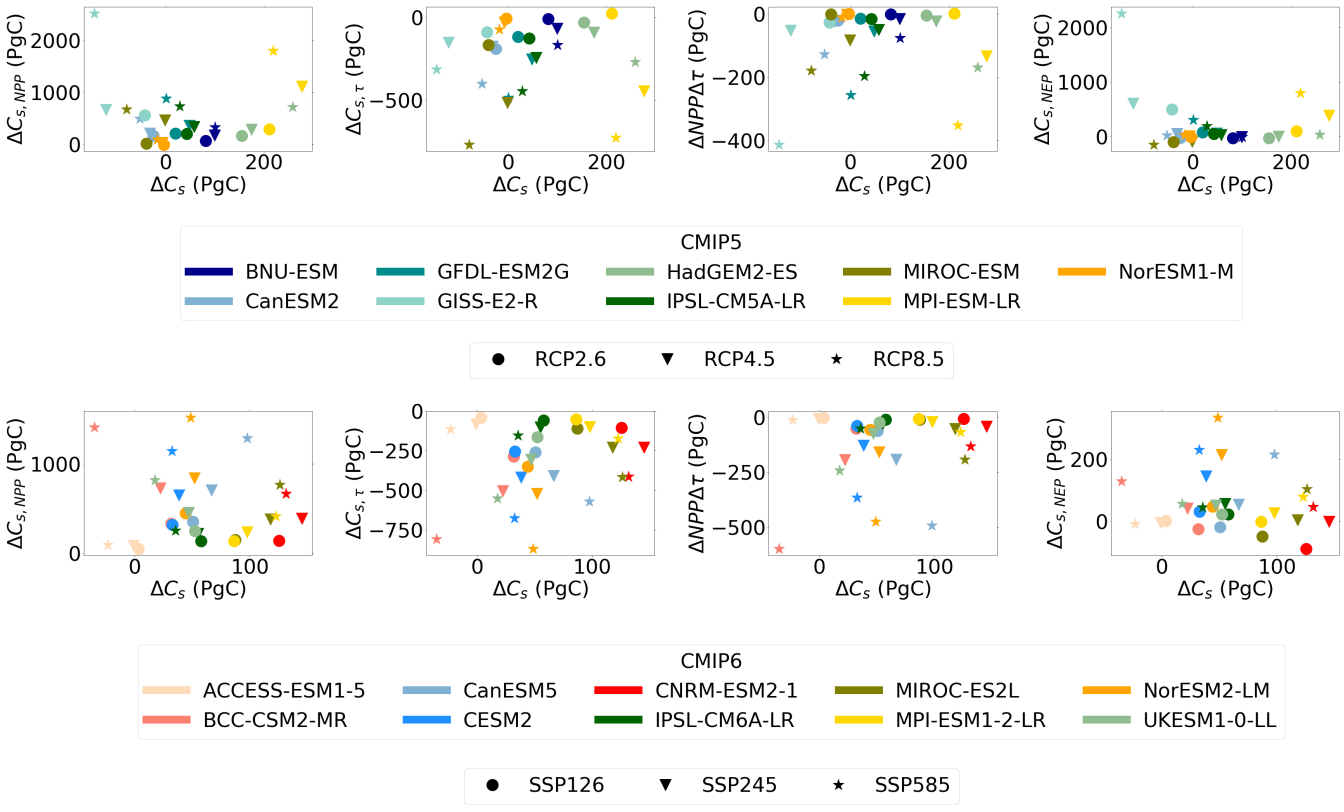

Figure A1. Scatter plot comparing the relationship between $\Delta C_{s,NPP}$, $\Delta C_{s,\tau}$, $\Delta\mathrm{NPP}\Delta\tau_s$, and $\Delta C_{s,\tau_{NEP}}$, each against ΔC_s, for CMIP5 (top row) and CMIP6 (bottom row) ESMs, for future scenarios *SSP126* and *RCP2.6*, *SSP245* and *RCP4.5*, *SSP585* and *RCP8.5*.

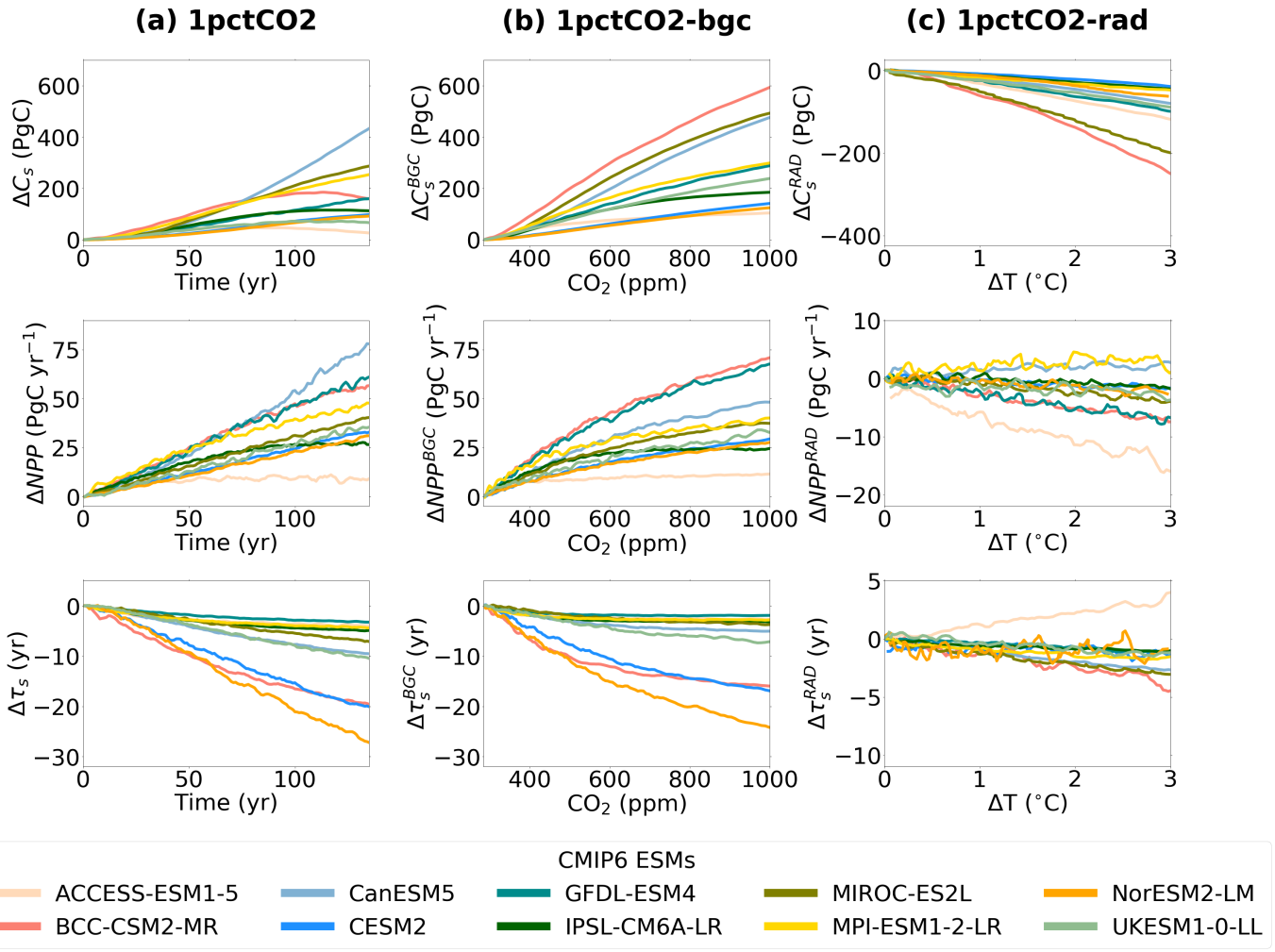

Figure A2. Timeseries of projected changes in Soil carbon (ΔC_s, top row) Net Primary Productivity (ΔNPP, middle row), and soil carbon turnover time ($\Delta\tau_s$, bottom row) in CMIP6 ESMs for the idealised simulations 1% CO_2 (left column), biogeochemically coupled 1% CO_2 (*BGC*, middle column) and radiatively coupled 1% CO_2 (*RAD*, right column).

Table A1. Table presenting the absolute (PgC) and relative (%) change in 21$^{\text{st}}$ century soil carbon for each CMIP5 model and the ensemble mean $\pm$ standard deviation, for each future RCP scenario.

Earth System Model	Absolute ΔC_s (PgC)			Relative ΔC_s (%)		
	RCP2.6	RCP4.5	RCP8.5	RCP2.6	RCP4.5	RCP8.5
BNU-ESM	81.4	99.7	100	11.6	14.2	14.3
CanESM2	-25.4	-32.7	-53.5	-1.65	-2.12	-3.47
GFDL-ESM2G	19.9	47.9	0.278	1.40	3.37	0.020
GISS-E2-R	-43.1	-122	-146	-1.92	-5.43	-6.50
HadGEM2-ES	154	174	258	13.9	15.6	23.2
IPSL-CM5A-LR	42.5	57.1	28.4	3.14	4.22	2.10
MIROC-ESM	-39.9	-1.53	-80.0	-1.55	-0.059	-3.11
MPI-ESM-LR	211	277	219	6.94	9.09	7.19
NorESM1-M	-3.94	-7.60	-17.7	-0.723	-1.40	-3.26
Ensemble mean	44.1	54.7	34.3	3.45	4.17	3.38
$\pm$ standard deviation	$\pm$ 84.2	$\pm$ 111	$\pm$ 127	$\pm$ 5.66	$\pm$ 6.97	$\pm$ 9.24

Table A2. Table presenting the change in 21st century NPP and τ_s for each CMIP5 model and the ensemble mean $\pm$ standard deviation, for each future RCP scenario.

Earth System Model	ΔNPP (PgC)			$\Delta\tau_s$ (yr)		
	RCP2.6	RCP4.5	RCP8.5	RCP2.6	RCP4.5	RCP8.5
BNU-ESM	4.52	11.7	21.9	-0.165	-1.36	-3.42
CanESM2	6.94	8.73	20.4	-2.95	-2.71	-6.23
GFDL-ESM2G	9.47	16.4	40.13	-1.53	-3.31	-6.38
GISS-E2-R	11.5	13.6	51.4	-2.26	-3.88	-8.03
HadGEM2-ES	10.4	18.2	45.5	-0.40	-1.24	-3.66
IPSL-CM5A-LR	10.4	16.9	37.0	-1.50	-2.91	-5.31
MIROC-ESM	0.350	9.98	14.4	-2.66	-8.32	-12.4
MPI-ESM-LR	-	26.6	43.0	-0.280	-5.00	-8.17
NorESM1-M	-0.388	2.25	6.94	-0.151	-0.645	-1.55
Ensemble mean	5.32	12.4	28.1	-1.26	-3.26	-6.13
$\pm$ standard deviation	$\pm$ 4.74	$\pm$ 7.42	$\pm$ 16.8	$\pm$ 1.13	$\pm$ 2.21	$\pm$ 3.03